Colloids and Surfaces B: Biointerfaces 256 (2025) 114986

Contents lists available at ScienceDirect

Colloids and Surfaces B: Biointerfaces

journal homepage: www.elsevier.com/locate/colsurfb

# Kraft lignin/polyurethane composites with enhanced mechanical strength, bioactive functionality, and superior wet wood adhesion

Maham Arif [a], Avishek Mallick Choudhury [b], Aleezay Anjum Ahmed [a], Vijay Singh Parihar [c], Md. Elias Uddin [d], Minna Kellomäki [c], Pralay Maiti [b], Rama Layek [a,*]

[a] LUT University, School of Engineering Science , Department of Separation Science, Mukkulankatu 19, Lahti 15210, Finland
[b] School of Materials Science and Technology, Indian Institute of Technology (Banaras Hindu University), Varanasi 221005, India
[c] Biomaterials and Tissue Engineering Group, Faculty of Medicine and Health Technology, Tampere University, Finland
[d] Department of Leather Engineering, Faculty of Mechanical Engineering, Khulna University of Engineering & Technology, Khulna 9203, Bangladesh

ARTICLE INFO

*Keywords:*
Polyurethane composite resin
Kraft lignin and castor oil
Bio-based additives
Excellent mechanical properties
Wet-state wood bonding strength
Antibacterial activity
Antioxidant activity

ABSTRACT

Conventional additives used in composite resins, widely employed in various industrial and domestic applications particularly in polymer composite films and wood adhesives, pose significant environmental and health concerns due to their petrochemical origins. To address this challenge, we developed a novel polyurethane (LPU) composite resin integrated with kraft lignin (KL) as a bio-based additive, exhibiting excellent multifunctional properties. The synthesis involved reacting poly(ε-caprolactone) diol and citric acid with 2,4-toluene diisocyanate, followed by the incorporation of KL and castor oil (CO) as reactive bio-additives to enhance the functionality of the LPU. CO not only improved the bio-content of the LPU but also facilitated the processability of KL during synthesis. The LPU was characterized using FTIR, WAXS, X-FESEM, and SS-CP-MAS $^{13}C$ NMR techniques. The LPU5 film exhibited a significantly higher tensile strength (8.1 ± 1.0 MPa) compared to the pure PU film (3.6 ± 1.5 MPa). The LPU15 wood adhesive demonstrated improved bio-content along with excellent shear strength and evident wood failure in wet environment, relative to pure PU. Furthermore, LPU composite resin mitigated the oxidative stress and also suppressed the proliferation of *Escherichia coli* (a Gram-negative bacterium), and *Staphylococcus aureus* (a Gram-positive bacterium) compared to pure PU. This study introduces a novel strategy for preparing LPU composite resin through the integration of bio-based additives, achieving enhanced bio-content, superior mechanical strength, wet wood-bonding ability, and improved bioactive properties such as antibacterial and antioxidant activity, thereby presenting a sustainable and reliable alternative to petrochemical-based constituents.

## 1. Introduction

Since its industrialization in 1937, polyurethane (PU) has become one of the most versatile polymers, widely used across various industries, including furniture, construction, automotive, textiles, and healthcare [1,2]. In 2021, the estimated worth of PU marketplace was $72.82 billion worldwide, with the projected compound annual growth rate between 2022 and 2023 is 4.3 % [3]. Generally, the synthesis of PU involves a polyaddition reaction in which either a diol or a polyol (R-OH) reacts with a di-isocyanate or poly-isocyanate (R-(N = C═O), resulting in urethane linkage (-NH-(C═O)-O-). PU composite resins formulated with additives are widely recognized for their exceptional properties, including rapid curing, durability, high mechanical strength, and excellent flexibility (i.e., large elongation at break), which are essential for diverse industrial applications such as protective films, foams, coatings, adhesives [4–7]. However, the continued reliance on petrochemical- or mineral-based additives in PU systems presents critical challenges. These conventional additives are often associated with toxicity, long-term environmental persistence, and a high carbon footprint due to their origin from non-renewable resources and their non-biodegradable nature [8,9]. Additionally, the urgent need to replace petrochemical-based additives arises from substantial evidence of their environmental persistence, contribution to greenhouse gas emissions, and potential toxicity to human health [10–12]. Subsequently, growing attention has been directed towards the development of bio-based additives for PU composite resin formulations as a

* Corresponding author.
*E-mail address:* rama.layek@lut.fi (R. Layek).

https://doi.org/10.1016/j.colsurfb.2025.114986
Received 31 May 2025; Received in revised form 19 July 2025; Accepted 24 July 2025
Available online 26 July 2025

promising solution. These bio-based additives are designed not only to mitigate environmental and health risks but also to increase the bio-based content and impart additional functionalities to PU composites. In this context, researchers have explored a variety of functional additives such as chain extenders, adhesion promoters, plasticizers, and reactive fillers, which are crucial for improving PU composite resin performance, while simultaneously reducing reliance on components derived from petroleum [2,13,14].

PU composite resins synthesized from biobased feedstock offer a promising substitute for petroleum-derived components due to their non-toxic nature, biodegradability, and reduced environmental impact. Concerning bio-resources, utilization of kraft lignin (KL) as a multifunctional bio-additive in PU systems stands out owing to its aromatic structure and reactive hydroxyl groups [15–18]. However, its direct use as an individual polyol in PU formulations often yields extremely rigid and brittle materials [19,20]. Even when used as a primary polyol in combination with other polyols such as PCL diol (poly ε-caprolactone diol) or CO (castor oil), issues such as agglomeration, poor dispersion, and compromised mechanical performance persist [21–24]. Moreover, its complex three-dimensional structure and steric hindrance reduce its reactivity with isocyanates, especially aromatic ones, thereby necessitating modifications to enhance its reactivity. However, such modifications often involve complex procedures, added costs, or sustainability concerns [25]. Furthermore, PU in wood adhesives and composite films also inherently lacks resistance to bacterial attack and oxidative degradation. Its carbon-rich soft segments provide favorable sites for bacterial colonization, leading to biofilm formation, enzymatic degradation, and adhesive failure under humid or high-contact conditions [26]. To mitigate these challenges, antibacterial and antioxidant functionalities have been introduced into PU systems, typically via inorganic nanoparticles such as Ag, Cu, or ZnO. However, these additives are not biobased and biodegradable and present concerns related to leaching, cytotoxicity, and environmental persistence [26,27]. Additionally, PU is also vulnerable to oxidative stress induced by heat, ultraviolet (UV) radiation, and atmospheric oxygen, resulting in chain scission and deterioration of mechanical properties over time [28]. Despite promising advances in using KL as an additive in PU composite resin formulations, significant challenges remain in enhancing its dispersibility and processability. These challenges hinder achieving satisfactory mechanical performance, including elongation at break and wood bonding strength under wet and humid conditions, as well as the effective expression of its bioactive (antioxidant and antibacterial) functionalities. This underlines the importance of optimizing KL incorporation into PU to improve mechanical and bonding performance under wet conditions and to fully utilize its bioactive functionalities.

The present study aims to address these challenges by synthesizing a novel PU composite resin exhibiting excellent mechanical, antibacterial, and antioxidant properties, along with superior wood adhesion strength in wet environments, via judicious integration of KL additive. The KL/PU composite resin was synthesized by reacting poly(ε-caprolactone) diol (PCL diol) and citric acid (CA) with 2,4-toluene diisocyanate (2,4-TDI), following by the addition of KL with CO (castor oil) as bio-based reactive additives. Each component plays a specific role in the synthesis of KL-additive integrated PU (LPU) composite with enhanced functionalities. PCL diol, TDI, and CA were selected for LPU synthesis due to their complementary properties. PCL diol is well known for its flexibility, biodegradability, and elastomeric characteristics, making it a valuable component for improving the mechanical strength of PU [29]. TDI exhibits high reactivity and forms strong urethane bonds, producing a robust polymer backbone [6]. Additionally, CA functions as a cross-linker, enhancing interfacial adhesion and mechanical performance of the synthesized PU [30]. Based on these advantages, we hypothesized that combining the functionalities of KL with PCL diol, TDI, CO, and CA in a PU-derived LPU composite resin would achieve a balance of flexibility and mechanical strength, resulting in overall required and satisfactory performance. Furthermore, during the LPU synthesis process, CO acts as a synergistic dual-purpose additive, both as a reactive component and as a medium that enhances the processability/dispersibility of KL. The synergistic presence of CO improves interaction between KL additive and the isocyanate reactants, thereby facilitating the incorporation of the KL additive into the PU composite through reactive blending [18,31–33]. In addition, CA, KL additive and CO are derived from natural resources, thereby increasing the sustainability and bio-content of the LPU composites. This research thus explores the synergistic use of KL additive with CO to enhance the processability of KL, which in turn substantially enhances the mechanical properties of LPU composite resin. To evaluate their potential as natural and effective antibacterial and antioxidant bio-additives, the prepared LPU composite films were tested against*Escherichia coli* and *Staphylococcus aureus* bacterial strains, as well as for their capacity to scavenge the DPPH (2,2-diphenyl-1-picrylhydrazyl) radical. Moreover, attributable to the chemical functionality and hydrophobic nature of KL, we hypothesize that the integration of KL into PU matrix can further enhance the mechanical strengths of LPU composite films and improve wood adhesion strength of the LPU composite resins under wet environments. Comprehensive characterization was focused on the physico-mechanical characteristics of the LPU composite resin and its performance as a wood adhesive in both dry and wet environments. By leveraging plant-based resources as additives, this research aims to contribute to the development of high-performance LPU composites, thereby addressing the polymer industry's increasing demand for environmentally safer additives.

## 2. Experimental procedure

### 2.1. Materials

Soft wood kraft lignin (KL) provided by the UPM under product name of BioPiva™ 100 (which has an acid value of 0.49 mmol/g and a hydroxyl value of 6.07 mmol/g) and originally derived from the industrially significant crop *Pinus taeda* (loblolly pine). KL was thoroughly ground into a fine powder with a mortar and pestle before use. PCL diol (poly ε-caprolactone diol) (with 2000 $gmol^{-1}$; average molecular weight), and citric acid (CA) both were obtained from Sigma-Aldrich in the U.S.A. Castor Oil (CO), triethylamine ($Et_3N$/TEA), 2,4-toluene diisocyanate (TDI), and xylene were procured from Merck, Germany.

### 2.2. Synthesis of kraft lignin-additive integrated polyurethane composite

To prepare KL-additive integrated PU (LPU) composites, 0.57 g of CA and 4.0 g of PCL diol were first mixed for 1 h in a 100 mL 3-neck round bottom flask, equipped with a nitrogen inlet, mechanical stirrer, and thermometer, and submerged in a silicone oil bath on a hot plate. Throughout the entire reaction, the mixture was continuously purged with nitrogen while maintaining a constant stirring speed of 130 rpm and a reaction temperature at 70 °C. Subsequently, 1.3 mL of TDI was added dropwise over a 10-minutes period, and the reaction continued for 3 h to form a pre-polymer. Following this, 2.66 g of CO was mixed with KL-additive at concentrations of 5 wt%, 10 wt%, and 15 wt% based on the total mass percentage with respect to all components and introduced into the reaction mixture to prepare LPU5, LPU10, and 167 LPU15 composite, respectively. The specific KL wt% was selected based on preliminary formulation trials aimed at achieving a gradual increase in KL-additive content while maintaining desirable phase compatibility and processability. Additionally, CO functions as a synergistic, dual-purpose additive: it acts as a reactive component that enhances the interaction between the KL additive and isocyanate reactants, and as a processing aid that improves the dispersion and processability of KL within the PU matrix [32]. Xylene was used as a solvent. The reaction continued for an additional 2 h and then 0.39 mL of TEA was introduced. The final LPU formulations were poured into separate Teflon dishes for curing to form composite films, and formulations were applied to wooden blocks for evaluation as wood adhesives. The samples were left

to cure at room temperature overnight. The identical process was followed to synthesize pure PU resin for comparison with LPU resin, except that KL additive was not included; the PU resin was cured following a similar procedure to produce films and applied to wood samples.

### 2.3. Preparation for bacterial dilution for antibacterial assay

Gram-positive S. aureus (ATCC 25923) and Gram-negative E. coli (ATCC 25922) strains were cultivated at 35 ± 1 °C in 5 mL of Tryptic-soy broth (TSB) for 24 h. The turbidity of the bacterial suspensions was adjusted to match the 0.5 McFarland turbidity standard, which is 1.5 x 108 CFU/mL. A saline dilution of ratio 1:1000 of the bacterial strains was prepared to yield approximately about 1.5 × 105 CFU/mL.

#### 2.3.1. Preparation of sample dilution

Since PU and LPU are hard polymeric materials, they do not dissolve/disperse in water. Thus, PU and LPU stock solutions were prepared by putting the material in a minimum amount of DMSO for 2–4 hrs and making up the volume with distilled water (to maintain the final concentration of DMSO at ~1 %). The preparation of KL stock was made in Mueller-Hinton Broth (MHB) of SRL CHEM. For the assay with *S. aureus* (ATCC 25923), KL, PU, and LPU polymer composites were prepared in the dilution range of (i) 0.1 mg/mL to 10 mg/mL, (ii) 10 mg/mL, and (iii) 10 mg/mL to 50 mg/mL, respectively, in MHB. For the experiment with *E. coli* (ATCC 25922), KL, PU, and LPU polymer composites were prepared in the dilution range of (i) 0.1 mg/mL to 20 mg/mL, (ii) 10 mg/mL, (iii) 25 mg/mL to 65 mg/mL, respectively, in MHB.

### 2.4. Characterization

The characterization of KL, PU, and LPU polymer composites was conducted using various advanced techniques.

#### 2.4.1. FT-IR Spectroscopic Analysis

In order to examine the presence of functional groups in the KL, PU, and LPU polymers a PerkinElmer Spectrum One model of Fourier-transform-infrared (FTIR) spectrophotometer (Waltham, MA, U.S.A) was used. Spectroscopic measurements were performed in the attenuated total reflection mode (ATR) at a resolution of 4 $cm^{-1}$ over the infrared range of 4000 $cm^{-1}$ to 400 $cm^{-1}$.

#### 2.4.2. WAXS Analysis

A Bruker AXS-D8 ADVANCE diffractometer operating at 40 kV with Cu Kα radiation, was used to undertake wide-angle X-ray scattering (WAXS) measurements of KL, PU, and LPU composite samples. All samples were scanned over a 2θ range of 5 ° to 60 ° with a step duration of 0.3 s and an increment rate of 0.015 °. The interplanar d-spacing values for each sample were calculated using Bragg's law $d = \lambda/2\sin(\theta)$ [34] to evaluate changes in molecular packing and segmental organization within the polymer matrix.

#### 2.4.3. X-FE-SEM Analysis

The fractured surfaces of PU and LPU polymer films were investigated by using cross-sectional field emission scanning-electron-microscopic study (X-FESEM). SEM, or scanning electron microscopic study was employed to analyze mechanically fractured wood adhesive surfaces using the JEOL JSM-7900F instrument.

#### 2.4.4. SS-CP-MAS $^{13}C$ NMR Analysis

A JEOL 500 MHz spectrometer (with model number SCZ500R, JEOL Resonance, made in Japan) was used to record the cross-polarization magic-angle-spinning 13-carbon NMR spectra (SS-CP-MAS $^{13}C$ NMR) of KL, PU, and LPU polymer samples in solid state by using a cross-polarization HXMAS probe at high-resolution at an 18 kHz spinning rate. As dry materials, the samples were placed in 3.2 mm zirconia rotors.

#### 2.4.5. Antibacterial Activity Analysis

MIC or the minimum inhibitory concentration of KL, PU, and LPU polymer composites was measured by using the broth microdilution assay via following the Clinical and Laboratory Standards Institute (CLSI) guidelines [35]. The dispersion of KL, PU, and LPU polymer composites was prepared by serial dilution in Mueller-Hinton Broth (MHB) in microcentrifuge tubes. The adjusted bacterial suspension (20 μL of 1.5 x $10^5$ CFU/mL) was added together in each well which holds 80 μL of sample to make up 100 μL of total volume. The bacterial growth was monitored after every one-hour interval at 600 nm by using a BioTek SYNERGY H1 microplate reader, under continuous shaking while incubating at 35 ± 1 °C for 24 h. The lowest concentration of the KL, PU and LPU composite films, indicating inhibition in bacterial growth, was taken as MIC of that sample.

#### 2.4.6. Antioxidant Activity Analysis

The pure PU and LPU composite films were subjected to UV–vis spectroscopy using a UV-3600 Plus spectrometer. The UV-3600 Plus Spectrometer was used to measure and compare the absorbance levels of the control and test all the samples after three hours of exposure to a 2,2-diphenyl-1-picrylhydrazyl (DPPH) solution in order to evaluate the antioxidant and radical scavenging capabilities of LPU. The absorbance was measured at 517 nm, the wavelength where DPPH exhibits maximum absorption.

#### 2.4.7. Mechanical Property Analysis

A UTM (Universal Tensile Machine) device (model number: Shimadzu, AG-IC 100 kN) was used to assess the mechanical characteristics of the PU and LPU polymer films and wood adhesive samples in both dry and wet states at 22 ± 2 °C, with a strain rate of 5 mm/min. Adhesive bonding tests were conducted using wooden blocks of 100 mm × 20 mm × 9 mm dimensions, in accordance with ASTM D906 standard and relevant literature reports [36–39]. After applying the prepared adhesives to the wooden blocks, they were left to dry completely for one day at room temperature. Following a 24-hour drying period, the glued wooden blocks were submerged in water for six hours at room temperature in preparation for the wet test. Throughout the immersion duration, the water's temperature was maintained at 22 ± 1 ∘C. To remove excess water, the wooden blocks were kept at room temperature. UTM device was then used to conduct lap-shear tests of both dry and wet samples. Each adhesive formulation was evaluated using five specimens per sample set, and the statistical mean value of these five measurements was reported.

## 3. Results and discussion

LPU composite resins with progressively higher KL-additive concentrations may enhance sustainability, as they are entirely derived from plant-based materials in the pulp industry. It was observed that the color of the composite films and adhesives gradually changed from brown (LPU5) to dark brown (LPU15) and required a shorter curing time with increasing KL-additive concentration. The characterization of the various LPU composite films and adhesives was carried out using FTIR, WAXS, Solid-State CP-MAS $^{13}C$ NMR analysis, mechanical testing, morphology studies, antibacterial, antioxidant and wood bonding performance. Fig. 1

## 4. FT-IR spectroscopic analysis

KL, PU, and LPU composites were subjected to FTIR analysis in order to assess the presence of various functional groups; the resulting spectra are shown in Fig. 2. The stretching vibrations of aromatic and phenolic -OH groups are responsible for the broad band seen in the FTIR spectrum of KL, which spans from 3000 to 3600 $cm^{-1}$ . Furthermore, C-H stretching vibrations from -$OCH_3$ and -$CH_3$-$CH_2$ as symmetric and asymmetric vibrational modes were detected at 2836 $cm^{-1}$ and 2935

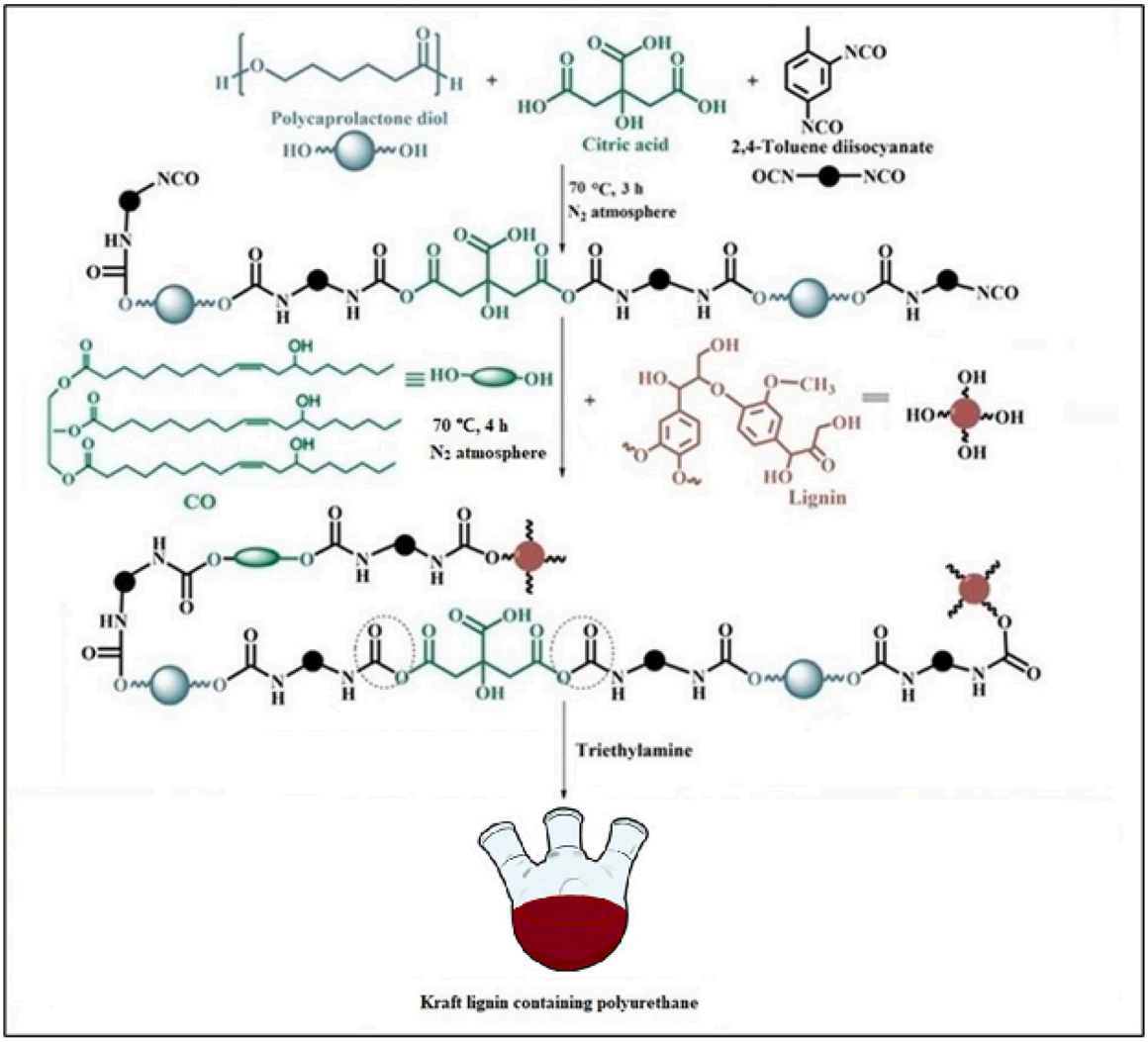


**Fig. 1.** Schematic representation of the synthesis of KL-integrated polyurethane (LPU) composite resin via incorporation of kraft lignin during the prepolymer phase.

$cm^{-1}$ , respectively. In the KL spectra a distinct peak at 1705 $cm^{-1}$ corresponds to unconjugated ketones or carbonyl (C═O) groups, and the aromatic C═C stretching vibrations are noted at 1598 $cm^{-1}$ and at 1513 $cm^{-1}$ , respectively. The asymmetric deformation of alkanes -$CH_3$ and -$CH_2$appears at 1457 $cm^{-1}$ , and a band around 1425 $cm^{-1}$ is linked to aromatic C═C stretching, accompanied by in-plane deformation of C-H bonds. Additionally, C-O stretching in secondary alcohols is indicated by a peak at 1267 $cm^{-1}$ , while aromatic alcohol or ether stretching vibrations are observed at 1214 $cm^{-1}$ . Aliphatic alcohol or ether stretching occurred at 1030 $cm^{-1}$ , with an aromatic C-H stretching band found out of plane at 817 $cm^{-1}$ [40]. In the PU spectrum, characteristic urethane bands are evident, particularly in the 3330–3340 $cm^{-1}$ region merged with -OH stretching vibration with the highest intense peak position at 3338 $cm^{-1}$ [41,42]. At 2930 $cm^{-1}$ and 2855 $cm^{-1}$ , symmetric and asymmetric C-$H_2$ stretching vibrations are seen, within the typical range for alkane C-H stretching (2920–2860 $cm^{-1}$). At around 2960 $cm^{-1}$ a weak shoulder band indicates the presence of C-$H_3$stretching from the fatty acid component of CO [41]. A C═O stretching vibration peak around 1722 $cm^{-1}$ is accredited to the urethane linkage, which normally appears within 1670–1730 $cm^{-1}$ range, depending on the polyol and diisocyanate used [41,43,44]. At 1600 $cm^{-1}$ a band links to C═C aromatic vibrations from TDI. The LPU spectra retains all the characteristic PU peaks, along with distinct shifts in several peak positions, confirming the successful integration of the KL-additive into the PU matrix. A slight peak shift in the urethane band O-H stretching region (3330–3340 $cm^{-1}$) was observed, from 3338 $cm^{-1}$ in PU to 3337 $cm^{-1}$ in LPU5, to 3333 $cm^{-1}$ in LPU10, and to 3332 $cm^{-1}$ in LPU15. This change implies that there is a hydrogen bonding interaction between the urethane groups in PU and the hydroxyl groups of KL. The C═O urethane stretching peak around 1730 $cm^{-1}$ broadens and demonstrates a slight shift from 1722 to 1728 $cm^{-1}$ from PU to LPU5, at 1729 $cm^{-1}$ in LPU10, and at 1726 $cm^{-1}$ in LPU15, respectively. This may be due to different bond environments of urethane C═O in LPU with respect to PU and also H-bonding interaction among urethane functional groups of LPU chains and KL additive. Additionally, the band near 1500 $cm^{-1}$ , attributed to aromatic C═C vibrations, shows a distinct peak at 1512 $cm^{-1}$ in LPU10, which was absent in PU, possibly indicating the integration of KL additive in the LPU10. Additionally, at 1160 $cm^{-1}$ a peak of C-O-C bond stretching was observed, suggesting the presence of ether linkages inherent to KL [45]. In the fingerprint region 500–1000 $cm^{-1}$ , few peaks emerged in the LPU spectra contributing to new vibrational modes might related to functional groups such as ether linkages (R-O-R) and phenolic groups (Ar-OH, Ar-O-R) from KL that were absent in PU. These spectral changes in LPU composites confirm the successful integration of reactive KL additive into the PU.

## 5. WAXS analysis

A wide-angle X-ray scattering (WAXS) study was conducted to investigate the structural characteristics of KL, PU, and LPU composites,

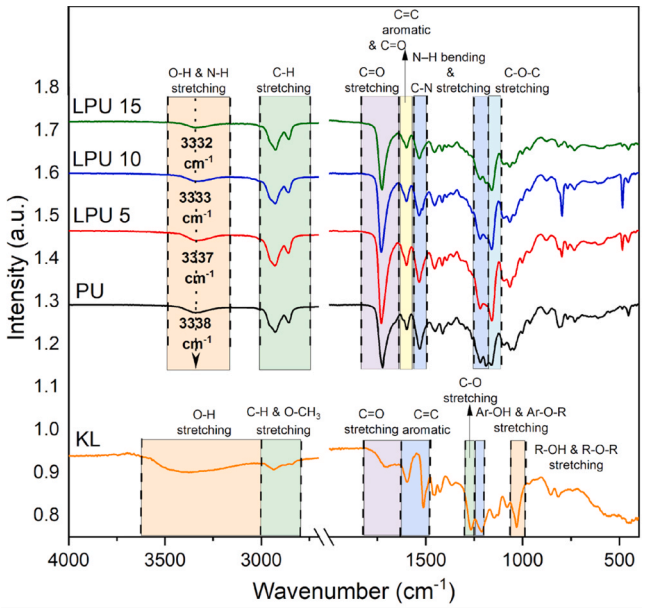


**Fig. 2.** FTIR spectra of KL, PU, and LPU composite resins, highlighting characteristic functional groups and structural modifications due to polymerization and kraft lignin integration into LPU composite resins.

and the subsequent diffractogram is presented in Fig. 3. The KL diffractogram exhibits characteristic broad peaks at 2θ = 20°-25° and 2θ = 40°-45°, indicating that KL is amorphous in nature and lacks well-defined crystalline diffraction patterns [46]. It is well established that PCL diol is a semicrystalline polymer whose crystalline structure is typically characterized by reflections from the (110) and (200) planes [47]. In contrast, PCL diol-based PU displays a characteristic broad diffraction peak at 2θ = 21.5 °, associated with the (110) plane of semi-crystalline regions of PCL-diol soft segment [47,48]. However, it is interesting to observe that the broad nature of the diffraction peak at 2θ = 21.5 °, related to 110 planes, is reduced in the LPU composites. Notably, upon the incorporation of KL, this peak becomes sharper and shifts slightly to higher 2θ values in LPU5, LPU10, and LPU15 composites. From the diffractogram, it is evident that in PU the interplanar

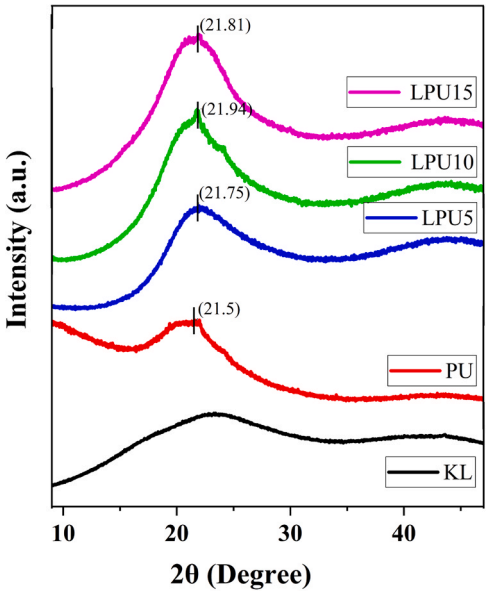


**Fig. 3.** WAXS patterns of KL, PU, and LPU composite resins, demonstrating structural differences and variations in phase morphology among the samples.

spacing is 0.4013 nm. In LPU5, LPU10, and LPU15, the diffraction peaks appeared at 2θ = 21.75 ° with d spacing = 0.408 nm, 21.94 ° with d spacing = 0.405 nm, and at 21.81 ° with d spacing = 0.407 nm, respectively. The overall decrease in d-spacing from pure PU to LPU composites (e.g. PU = 0.413 nm to LPU15 = 0.407 nm) indicates tighter molecular packing, particularly within the soft segment domains, suggesting the formation of more ordered crystalline structures. This densification is attributed to enhanced hydrogen bonding interactions between the hydroxyl groups of KL and the urethane linkages, which restrict chain mobility and reduce intermolecular distances. However, in LPU15, a slight decrease in 2θ (from 21.94 ° to 21.81 °) was observed compared to LPU10, which may be due to saturation of nucleation sites or some aggregation of KL at higher content. Furthermore, the increased sharpness of the crystalline peaks in the LPU samples suggests enhanced crystallization of PCL diol segments in the presence of KL, which may act as a nucleating agent and promote a higher degree of segmental ordering and more defined soft segment crystalline domains, particularly in the PCL diol phase. Additionally, the appearance of a minor broad peak around 2θ = 44 ° in all LPU samples indicates the presence of amorphous KL domains within the PU matrix [49].

## 6. Solid state CP-MAS $^{13}$C NMR analysis

To characterize the molecular structure, polymer morphology, and structural interactions within PU and LPU composites, CP-MAS $^{13}$C NMR spectra were recorded, and results shown in Fig. 4(a-e). These spectra, consistent with established literature values [50], confirm the successful integration of KL additive into the PU matrix and demonstrate its influence on composite properties. According to literature references [51–54], in Fig. 4a, the solid-state CP-MAS $^{13}$C NMR spectrum of KL shows a complex array of peaks in the range of 0–200 ppm, corresponding to its structural components. Notably, the intense peak of the methoxy group (-$OCH_3$) appears at 56 ppm, while peaks below 56 ppm correspond to aliphatic $CH_2$ and $CH_3$ groups, including signals at 34.21 ppm, 29.14 ppm, and 11.21 ppm. As reported in the literature, peaks between 60 and 85 ppm arise from α-, β-, and γ-carbons in the β-O-4 linkages, such as Cγ-OH, Cα-OH, and Cβ. However, the peaks appearing between 100 and 127 ppm arise from aromatic C-H positions, peaks between 127 and 140 ppm correspond to C-C positions, and peaks between 140 and 160 ppm are linked to C-O positions [51]. In the aromatic region (110–150 ppm), various peaks correspond to guaiacyl (G) units, including the C3 and C4 carbon peak at 148.43 ppm, C1 at 131.63 ppm, C6 at 124.07 ppm, and C2 at 108.96 ppm. Additionally, the carbonyl region exhibits a peak at 183.36 ppm, corresponding to carboxyl and conjugated carbonyl functionalities, further confirming the complex aromatic nature of KL [55].

In the PU spectrum (Fig. 4b), the aliphatic region (0–50 ppm) displays several distinct peaks, ranging from 8.66 to 46.69 ppm, originating from the polyol soft segment. Characteristic peaks at 8.66, 17.43, 25.93, 28.90, and 32.27 ppm correspond to methylene and other aliphatic carbons in the PU and PCL diol structure. A peak at 34.28 ppm is linked with soft-segment carbon in line with urethane linkages, however, a slightly smaller peak at 46.69 ppm displays the methylene carbon atoms in the hard segment of TDI. The methylene carbon adjacent to the urethane nitrogen in the TDI hard segment is slightly deshielded by the electron-withdrawing urethane group, resulting in a chemical shift at around 46 ppm. The 50–100 ppm region reflects carbons typically bonded to oxygen or nitrogen, such as in amines (C-N), alcohol (-OH), and in ethers (C-O-C). In the structure of PCL diol, characteristic peaks include the carbonyl carbon (-O-C═O-$CH_2$) of the ester group at 173.15 ppm, and a peak at 64.30 ppm corresponding to the methylene carbon contiguous to oxygen (-O-$CH_2$) in the polyester polyol (PCL diol) chains [56]. CO exhibits aliphatic carbon peaks in the 14–35 ppm range, with glycerol backbone peaks observed between 62 and 74 ppm and hydroxyl groups appearing between 65 and 75 ppm. These peak shifts indicate successful incorporation and interaction of CO

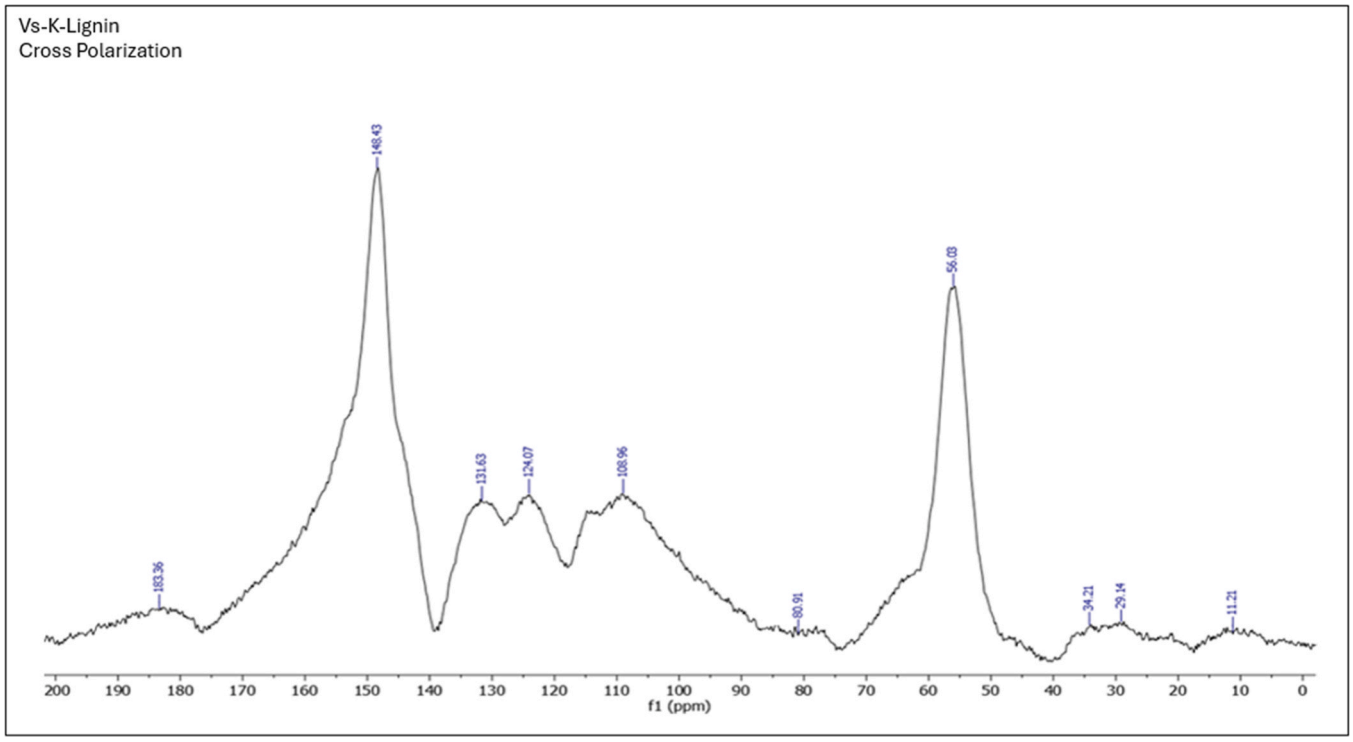


**Fig. 4a.** Solid-state Cross-Polarization Magic Angle Spinning $^{13}C$ NMR spectra of pure KL, recorded at 125 MHz, illustrating the chemical environment and structural features of carbon atoms within KL.

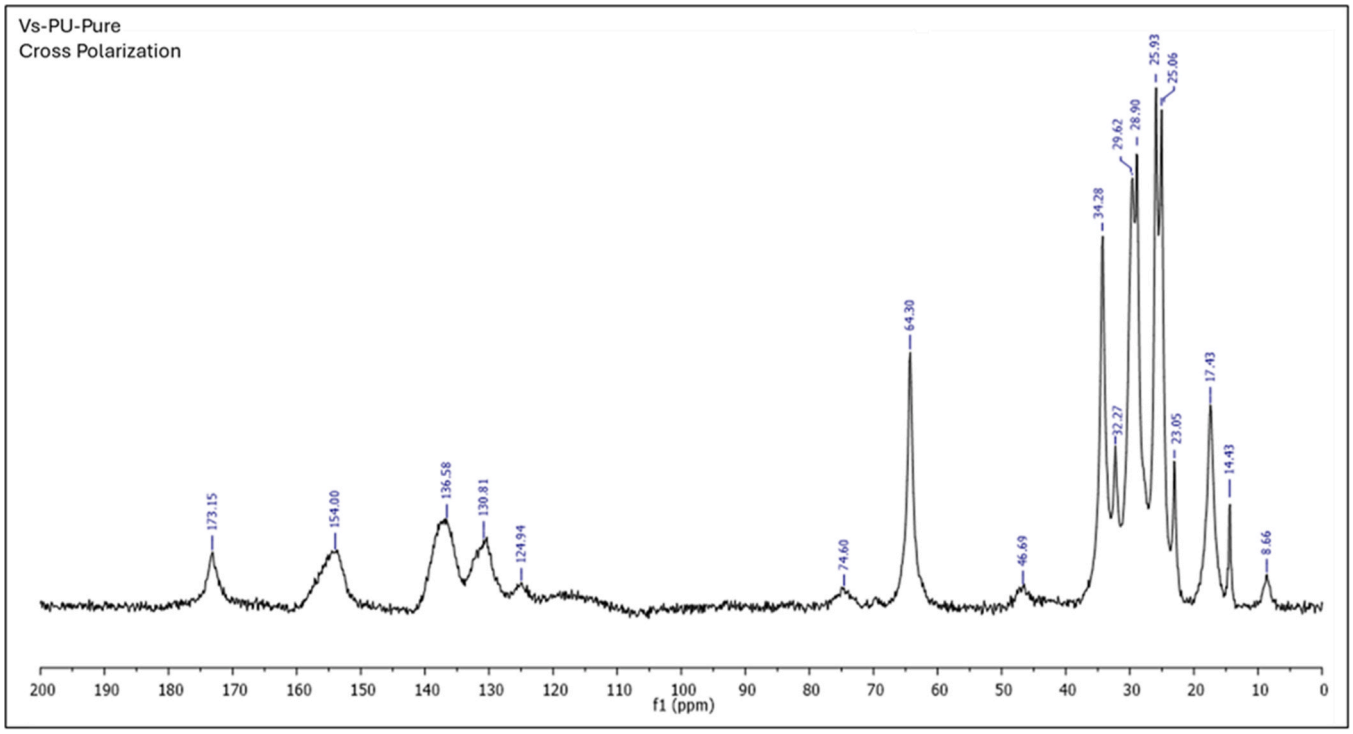


**Fig. 4b.** Solid-state Cross-Polarization Magic Angle Spinning $^{13}C$ NMR spectra of pure PU, recorded at 125 MHz, illustrating the chemical environment and structural features of carbon atoms within the polyurethane matrix.

within the PU matrix [57]. In the 100–150 ppm region, peaks are assigned to aromatic and olefinic carbons, with three primary signals between 120 and 140 ppm. Specifically, the peaks at 124.94 ppm and at 130.81 ppm are assigned to the protonated aromatic carbons of TDI, likely reflecting conformational variations in the solid state, while at 136.58 ppm the peak corresponds to quaternary ring carbons of TDI. In the 150–200 ppm region, peaks typically correspond to aromatic carbons in deshielded environments or those with electron-withdrawing substituents [58]. Two prominent peaks at 154 ppm and at 173.15 ppm in the carbonyl region, which is shown in Fig. 4b,

corresponds to carbonyl carbons likely from urethane linkages and carboxy carbons, respectively. These signals confirm the existence of TDI units, CO, and PCL diol, in the PU matrix, underscoring its complex molecular structure.

The successful integration of KL additive into the PU is confirmed by the SS-CP-MAS $^{13}C$ NMR spectra of the LPU composites. In the LPU spectrum (Fig. 4c-e), distinct peaks observed in the 50–60 ppm, 125–135 ppm, and 145–150 ppm regions indicate the incorporation of specific KL additive carbon environments into the PU. For instance, in LPU5 (Fig. 4c), the peak at 55.36 ppm is credited to the KĹs methoxy carbons, whereas the peak at 128.40 ppm relates to aromatic carbons, indicating the presence of aromatic rings in KL phenylpropane units. At 147.57 ppm a peak is associated with oxygenated aromatic carbons, such as those in phenolic hydroxyl groups (C-OH) or ether linkages (C-O-C), which is characteristic of KL. In LPU10 (Fig. 4d), a peak at 55.10 ppm is similarly designated to methoxy carbons, with the peak at 128.49 ppm corresponding to aromatic carbons and peak at 147.96 ppm is attributed to oxygenated aromatic carbons. In LPU15 (Fig. 4e), the peak at 55.90 ppm represents methoxy groups (-$OCH_3$), the peak at 128.51 ppm originates from aromatic rings in KL phenylpropane units, and the peak at 147.75 ppm is associated with phenolic hydroxyl groups (C-OH) and ether linkages (C-O-C). The observed peak shift from 124.94 ppm in the PU spectrum to 128.40 ppm, 128.47 ppm, and 128.51 ppm in the LPU5, LPU10, and LPU15 spectra, respectively, is attributed to the chemical interactions between functional groups of the KL and PU composite. These shifts are caused by changes in hydrogen bonding and the compatibility of KL within the composite. Additionally, increased phase separation at higher KL content and variations in cross-linking density can alter the chemical environment around the carbon atoms, further contributing to these shifts. Moreover, the peaks in the 145–150 ppm region such as those from phenolic hydroxyl groups (C-OH) and ether linkages (C-O-C) which were not present in the pure PU spectrum further confirms the incorporation of the KL additive in LPU.

## 7. Antibacterial activity analysis

Antibacterial properties of KL, PU, and all LPU composites were evaluated against a Gram-negative bacterium, *Escherichia coli* (ATCC 25922), and a Gram-positive bacterium, *Staphylococcus aureus* (ATCC 25923), using a broth microdilution method. Bacterial growth was monitored over a 24-hour period, and the results are shown in Fig. 5a-b and Table 1, respectively. As shown in Fig. 5a-b, the pure PU sample against both *E. coli* and *S. aureus*bacterial strains exhibited a typical sigmoidal bacterial growth curve, confirming its chemically inert nature and lack of inherent antibacterial properties. These findings are consistent with previous studies reporting that conventional PU materials lack biocidal activity unless they are chemically modified or reinforced with antibacterial fillers [26,27]

In contrast, KL exhibited concentration-dependent antibacterial behavior against both bacterial strains Gram-negative *E. coli* and Gram-positive *S. aureus*. At lower concentrations (e.g., 0.1 mg/mL), KL showed no antibacterial activity against *E. coli*. However, at its MIC value (10 mg/mL), bacterial growth was completely inhibited, indicative of inhibitory effects attributed to phenolic hydroxyl groups capable of interacting with bacterial membranes. A similar trend was observed against *S. aureus*, where moderate inhibition was noted at 1 mg/mL, but the bacterial growth was fully suppressed to 10 mg/mL. The incorporation of KL into the PU polymer significantly improved its antibacterial efficacy. The MIC of LPU5 against *S. aureus* was not observed within the tested concentration range of 10–50 mg/mL. Although it did not completely inhibit bacterial growth, the successive concentrations of LPU5 not only reduced the bacterial growth kinetically but also delayed the onset of the log phase, indicating partial inhibitory behavior. Against *S. aureus,* LPU10 and LPU15 showed complete inhibition at 35 mg/mL and 25 mg/mL, respectively. This could be because of the increased structural rigidity and limited porosity of the LPU15, which may hinder the growth of bacterial cells. Against *E. coli*, LPU composites demonstrated relatively lower yet significant antibacterial effects. Among the composites, LPU5 demonstrated antibacterial activity at 35 mg/mL, whereas LPU10 and LPU15 exhibited substantial and dose-dependent

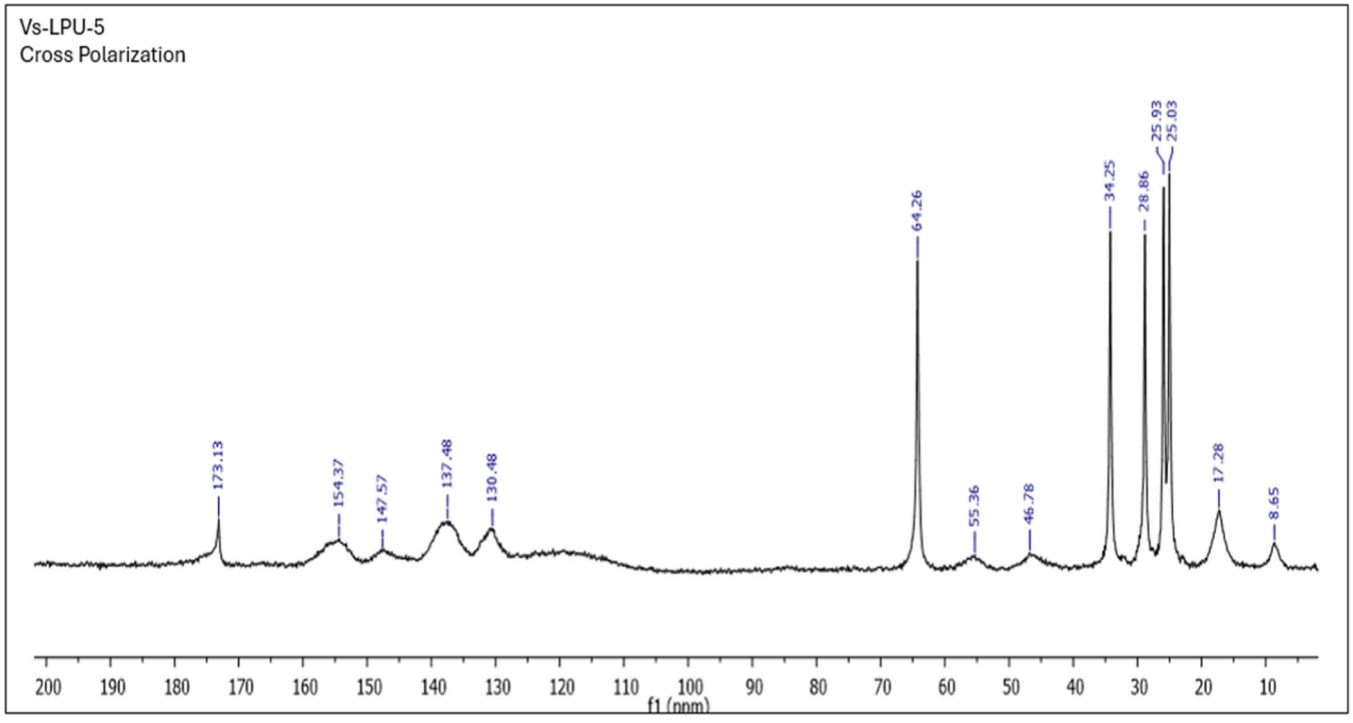


**Fig. 4c.** Solid-state Cross-Polarization Magic Angle Spinning $^{13}C$ NMR spectra of LPU5, recorded at 125 MHz, illustrating the chemical environment and structural features of carbon atoms within the 5 wt% KL-additive integrated polyurethane composite.

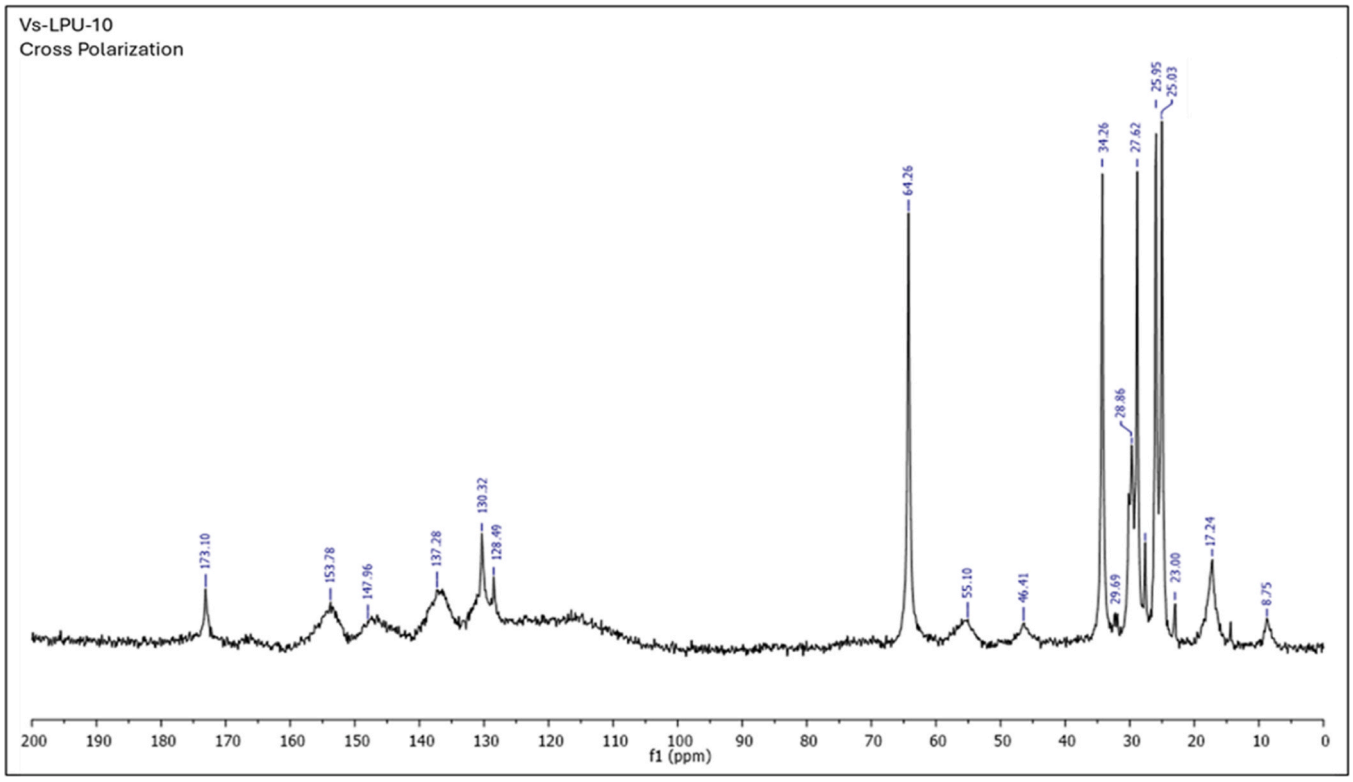


**Fig. 4d.** Solid-state Cross-Polarization Magic Angle Spinning $^{13}C$ NMR spectra of LPU10, recorded at 125 MHz, illustrating the chemical environment and structural features of carbon atoms within the 10 wt% KL-additive integrated polyurethane composite.

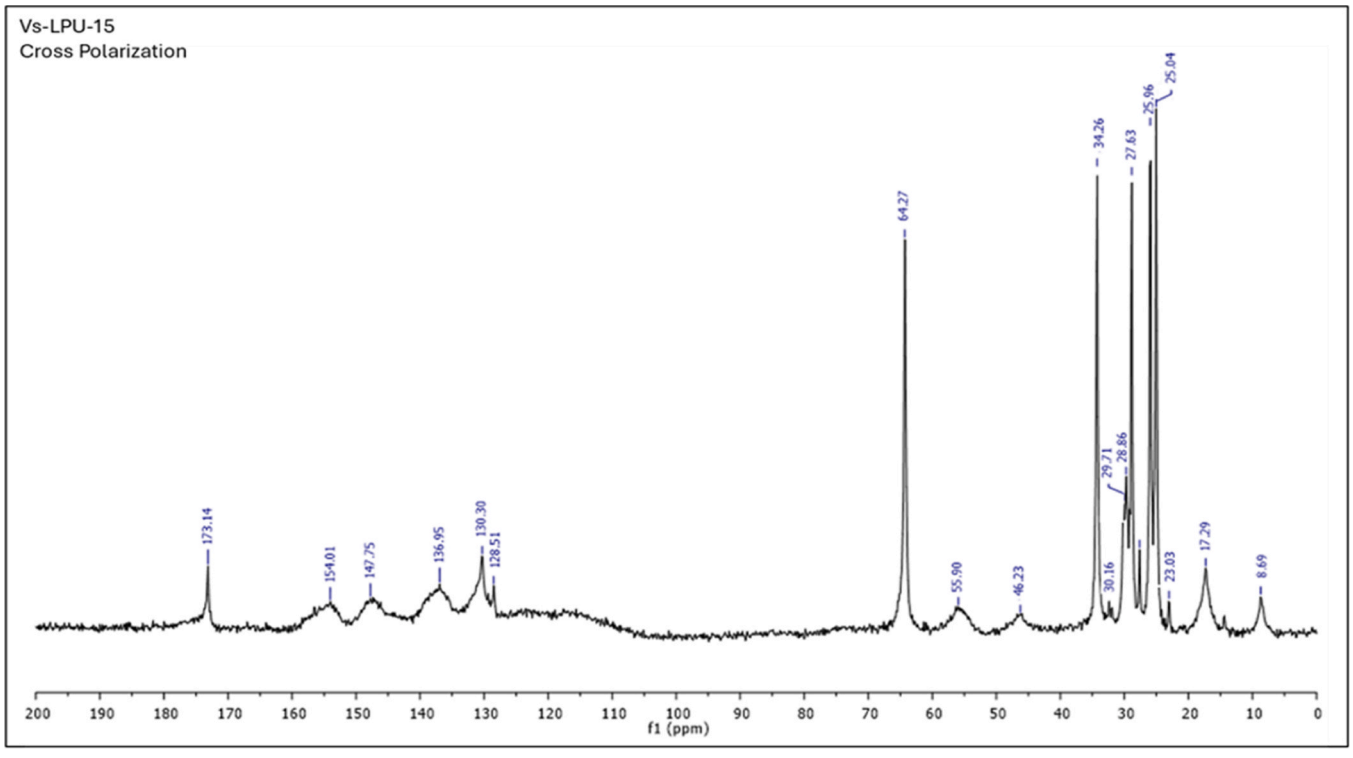


**Fig. 4e.** Solid-state Cross-Polarization Magic Angle Spinning $^{13}C$ NMR spectra of LPU15, recorded at 125 MHz, illustrating the chemical environment and structural features of carbon atoms within the 15 wt% KL-additive integrated polyurethane composite.

inhibition of bacterial growth. LPU10 at 25 mg/mL completely suppressed *E. coli* proliferation entirely over 24 h, while LPU15 showed even more pronounced inhibition at 25 mg/mL. This enhanced antibacterial behavior is attributed to the integration of KL redox-active moieties within the PU matrix, facilitating gradual release and sustained contact with bacterial cells [59,60]. The phenolic and quinone-like

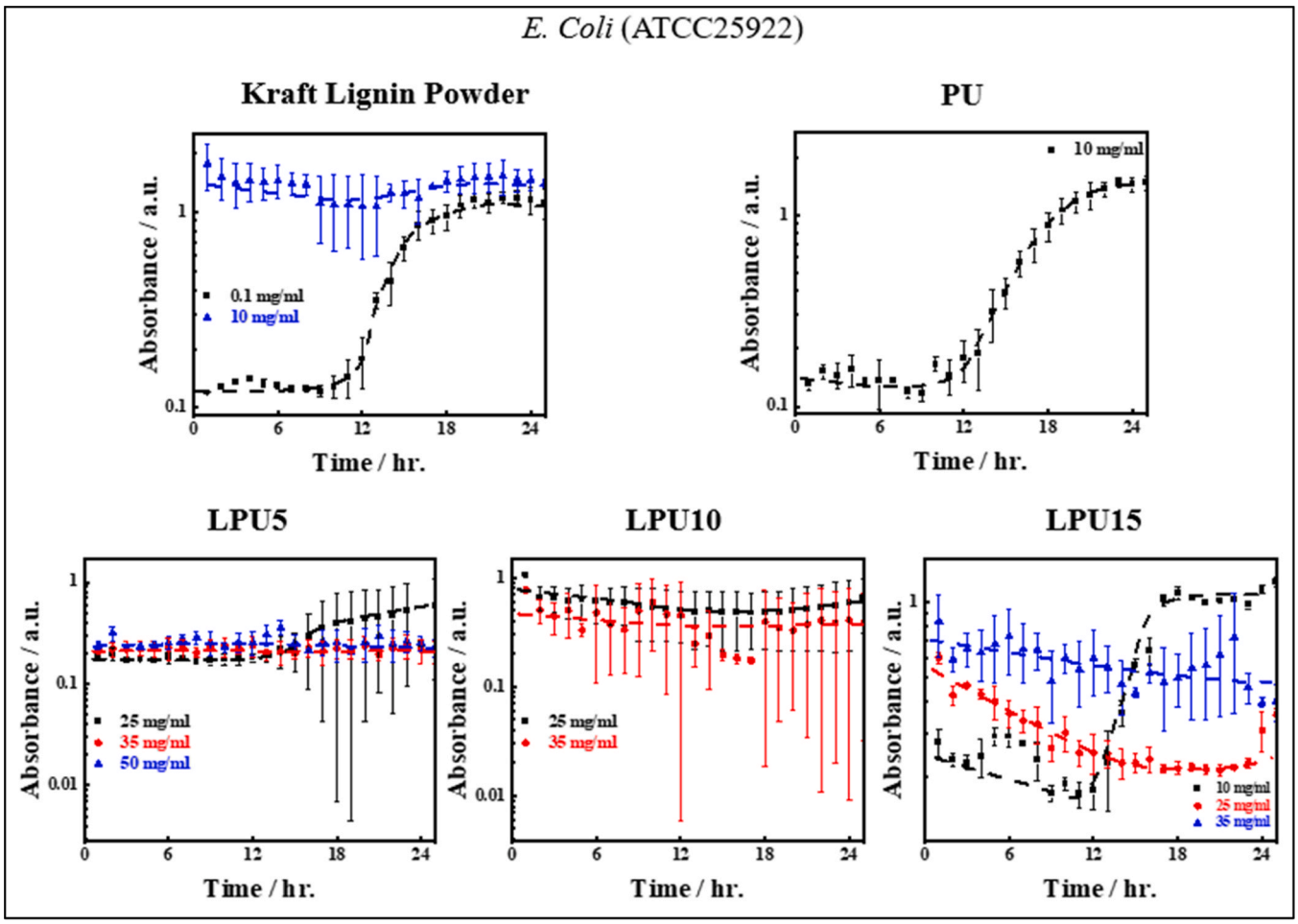


**Fig. 5a.** Assessment of antibacterial performance of KL, PU, and LPU composite resins against *E. coli* bacterium, illustrating material-specific inhibition effects.

**Table 1**
Minimum Inhibitory Concentration (MIC) of KL and LPU composite films against two control bacterial strains, demonstrating the antibacterial efficacy and comparative inhibition thresholds of the tested samples.

| Microorganisms | MIC (mg/mL) | | | |
|---|---|---|---|---|
| | KL | LPU composite films | | |
| | | LPU5 | LPU10 | LPU15 |
| *E. coli* (ATCC 25922) | 10 | 35 | 25 | 25 |
| *S. aureus* (ATCC 25923) | 10 | > 50 | 35 | 25 |

structures in KL are known to induce oxidative stress, disrupt membrane permeability, and inhibit enzymatic pathways in Gram-negative bacteria such as*E. coli*[61]. Furthermore, the differential susceptibility between*E. coli* and *S. aureus* is likely due to differences in cell wall structural, with Gram-negative bacteria being more vulnerable to phenolic-induced oxidative damage compared to Gram-positive *S. aureus*bacteria, with a thicker peptidoglycan layer [62]. The antibacterial property of KL in PU wood adhesives adds functional importance by inhibiting bacterial growth at the bonded interface, enhancing the durability and hygiene of wood products. This is particularly beneficial in moisture-exposed or high-contact environments, reducing the risk of bio-deterioration and extending service life.

## 8. Antioxidant activity analysis

The antioxidant potential of pure PU and all LPU composite films was investigated using the DPPH (2,2-diphenyl-1-picrylhydrazyl) free radical scavenging assay technique at 3-hour interval and monitored by UV–vis absorption spectroscopy. Fig. 6a-b shows the characteristic absorption curves of DPPH radicals, with a peak centered around 517 nm. The control (DPPH without any sample) exhibited the highest absorbance, reflecting the stability of the radical. Upon addition of PU and LPU samples, a gradual decline in absorbance was observed, indicating radical scavenging activity. Notably, the decline in absorbance intensified with increasing KL content, which is visually represented in the bar chart (Fig. 6b). Among the composites, LPU15 demonstrated the most pronounced antioxidant effect, followed by LPU10 and LPU5, whereas pure PU showed minimal activity, only slightly lower than the control. These results corroborate the previous literature reports that highlight the intrinsic antioxidant capacity of KL due to its rich content of phenolic hydroxyl groups, which are capable of donating hydrogen atoms to neutralize free radicals [63,64]. The trend observed in this study indicates that the integration of KL into the PU significantly enhances radical scavenging efficiency, and the effect is proportional to the KL loading. The reduced absorbance at 517 nm for LPU15 corresponds to an increased radical scavenging activity (RSA) of approximately 61 %, in contrast to PU, which showed less than ~7 % RSA. This improvement can be attributed to the intrinsic antioxidant properties of the KL additive and its effective dispersion within the PU, allowing its redox-active sites to remain accessible for antioxidant interactions via an electron transfer mechanism that reduces DPPH• to DPPH. Hence, the overall findings suggest that the antioxidant activity of LPU helps stabilize wood adhesives by scavenging free radicals, which can delay oxidative degradation. This can enhance the aging resistance of the adhesive, contributing to longer-lasting wood composites under environmental

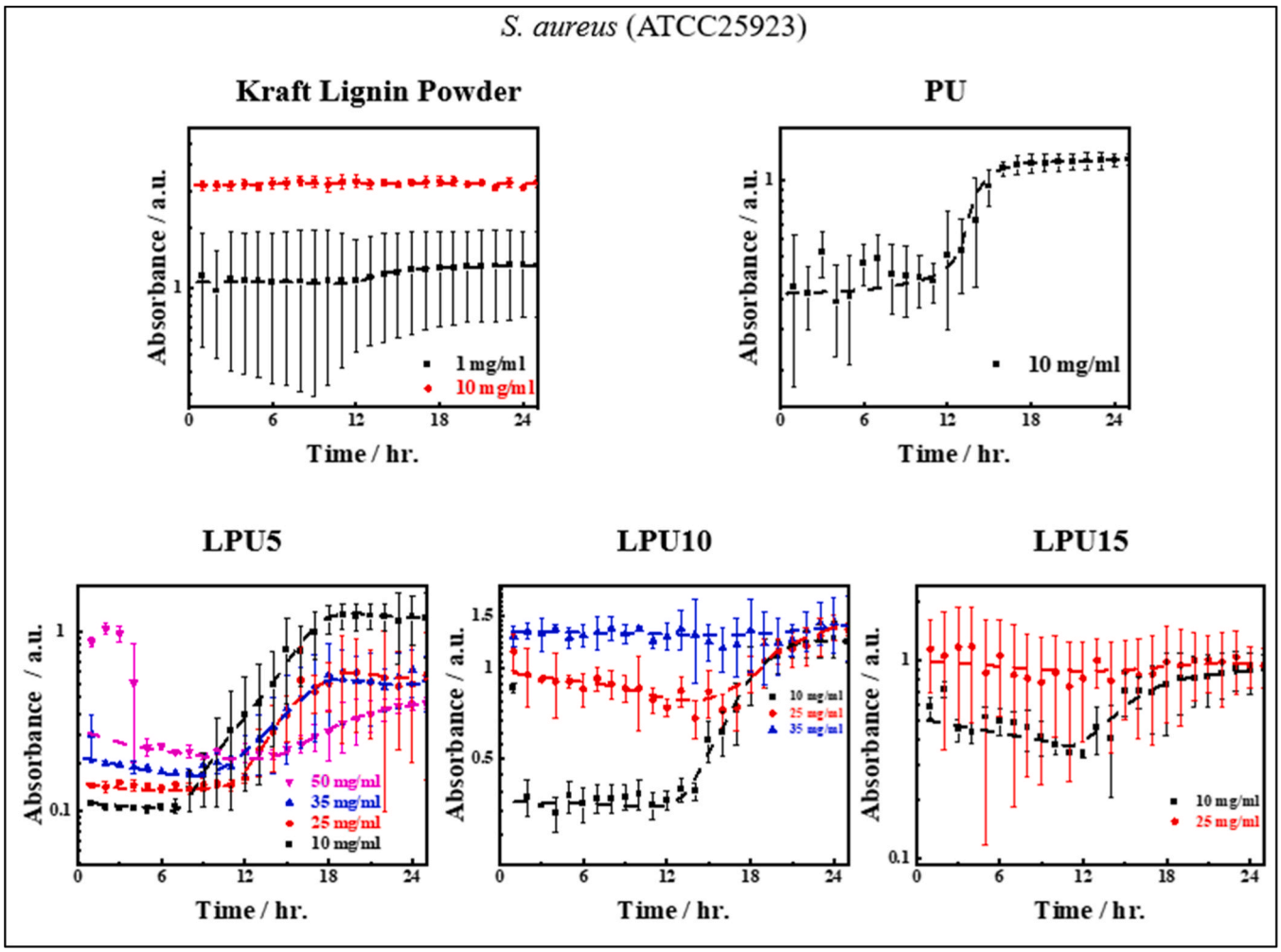


**Fig. 5b.** Assessment of antibacterial performance of KL, PU, and LPU composite resins against *S. aureus* bacterium, illustrating material-specific inhibition effects.

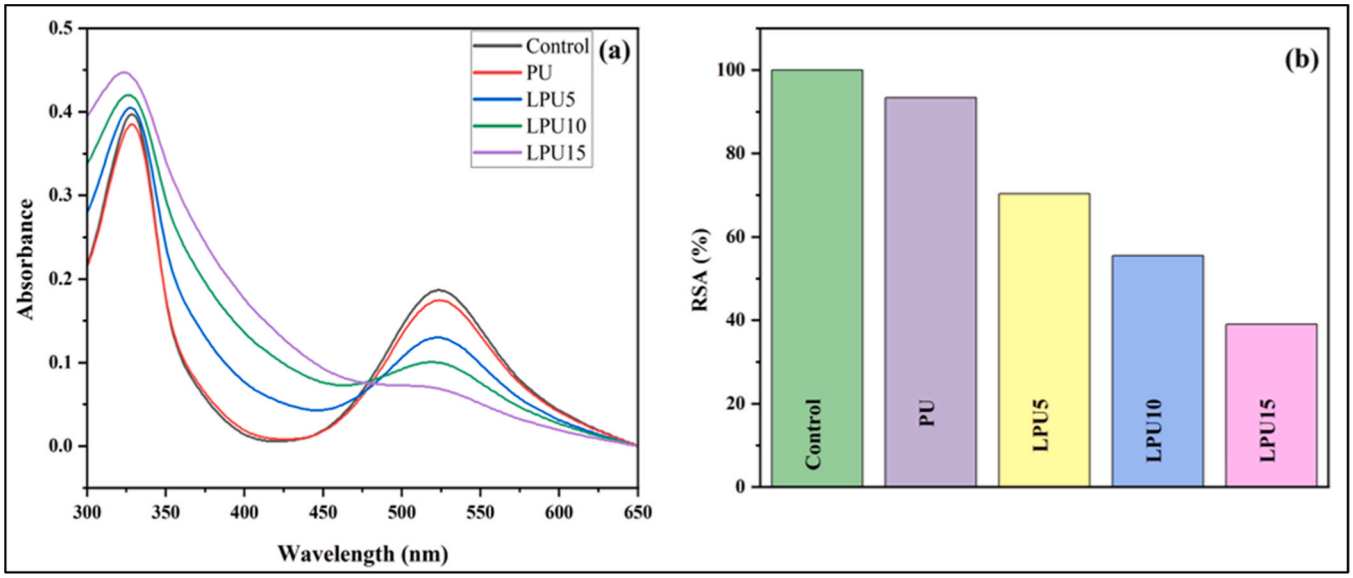


**Fig. 6.** Antioxidant activity of PU and LPU composites: (a) UV–vis absorption spectra illustrating DPPH radical scavenging behavior, and (b) bar chart showing absorbance values at 517 nm, indicating the comparative antioxidant efficiency of the samples.

stress.

## 9. Mechanical property of composite films

The stress-strain curves of PU and LPU composite films are displayed in Fig. 7(a-d) to examine the mechanical performance of the prepared composite films. The PU polymer film's tensile strength was 3.6 ± 1.50 MPa while the elongation at break was 1120 ± 35 %. In the LPU5 composite film the tensile strength was significantly observed at 8.10 ± 1.0 MPa, whereas the elongation at break was 815 ± 45 %. In the LPU10 and LPU15 composite films, the tensile strength was 6.0 ± 0.30 MPa and 5.8 ± 0.20 MPa, respectively, and the elongation at break was 820 ± 40 % and 900 ± 50 %, respectively. This trend is likely due to the increased rigidity and brittleness in LPU composite associated with higher KL content. The Young's modulus value of the PU film was noted at 133 ± 15 MPa, while for the LPU5 and LPU10 composite films, it was recorded at 245 ± 20 MPa and at 325 ± 12 MPa, respectively. However, in the LPU15 composite film, a slightly lower Young's modulus value at 234 ± 10 MPa was observed. It should be noted that at low KL concentration (5 wt%), the majority of the reactive KL additive is likely to be integrated into the PU polymer chain. However, as the KL concentration increases (10 wt% and 15 wt%), a fraction of the KL additive becomes incorporated into the PU chain, while another fraction accumulated and remained as a filler within the LPU10 and LPU15 composite films. The mechanical performance of the LPU5 composite film shows a significant enhancement compared to PU film. The tensile strength increased to 8.10 ± 1.0 MPa from 3.6 ± 1.50 MPa, and at the same time the Young's modulus increased to 245 ± 20 MPa from 133 ± 15 MPa. However, the strain at break decreased to 815 ± 45 % from 1120 ± 35 %. This enhancement in mechanical properties can be explained by the stronger intersegmental interactions and improved crystallization behavior observed from FTIR and WAXS analyses, which correlate well with the increased tensile strength and stiffness of the LPU composites, indicating more efficient stress transfer due to better polymer chain packing.

In the LPU10 and LPU15 composite films, the presence of KL additive as a filler enhanced rigidity and Young's modulus. However, these formulations also exhibit an unusually high elongation at break. This behavior can be explained by the "ball-bearing" effect of the KL filler. During tensile testing, the KL additive serves a dual role. On one hand, it transfers the load to the KL particles from the polymer matrix, thereby increasing rigidity and Young's modulus. On the other hand, it facilitates the PU chains sliding over the KL surfaces, introducing a plasticizing effect. This phenomenon is similar to what is observed in other KL-integrated systems [65]. In LPU15, the plasticizing effect might be more pronounced, leading to a further decrease in the Young's modulus value and tensile strength value while simultaneously increasing the elongation at break as compared to LPU10.

## 10. X-FESEM studies of composite films

To understand the cross-sectional morphologies of pure PU and LPU composite films and their structure, X-FESEM was performed, and the images are presented in Fig. 8. The pure PU film exhibits a continuous, smooth cross-sectional surface, while the LPU composite films display an uneven, rough surface with a highly aggregated particle-like structure. [66]. InFig. 8a, the pure PU film exhibits a smooth and uniform fractured surface, characterized by fine lines. However, in LPU5 (Fig. 8b), small

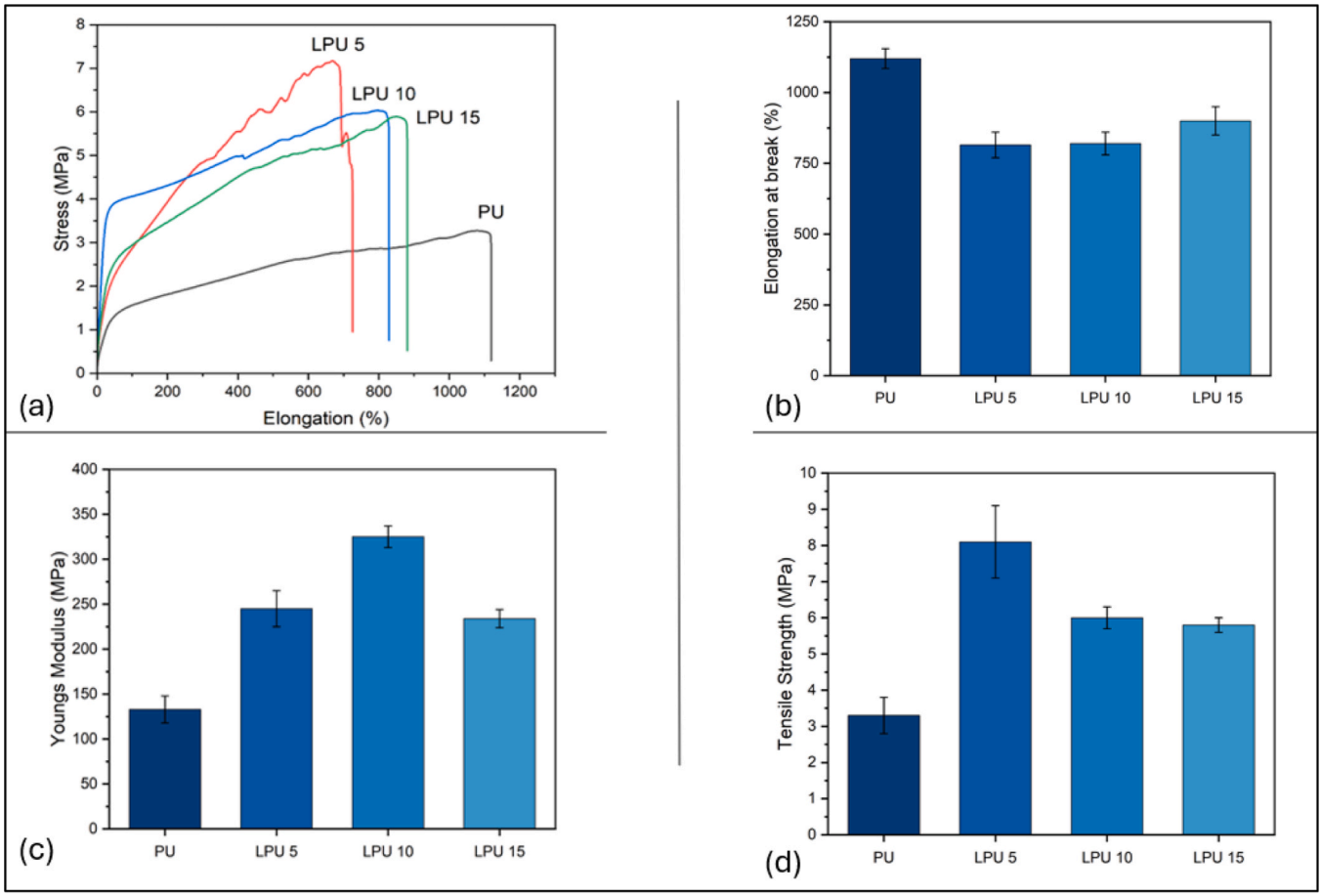


**Fig. 7.** Mechanical properties of PU and LPU composite films: (a) stress-strain behavior showing tensile stress (MPa) and elongation (%), (b) elongation at break (%), (c) Young's modulus (MPa), and (d) tensile strength (MPa), highlighting the effect of KL incorporation on mechanical performance.

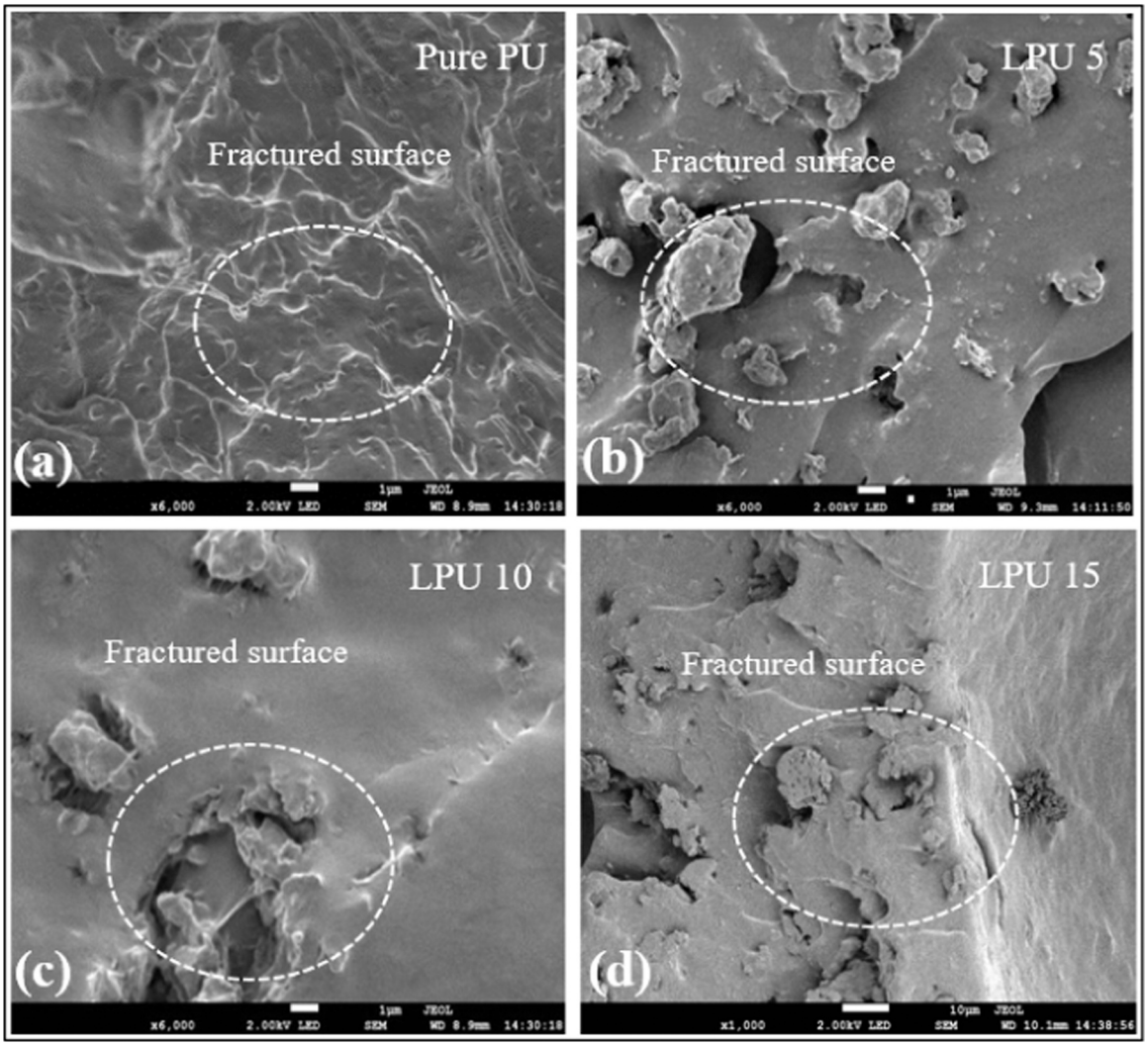


**Fig. 8.** FE-SEM images of PU and LPU composite films showing fractured surface morphology: (a) PU (b) LPU5 (c) LPU10 (d) LPU15, illustrating the influence of KL incorporation on microstructural morphology and fracture characteristics.

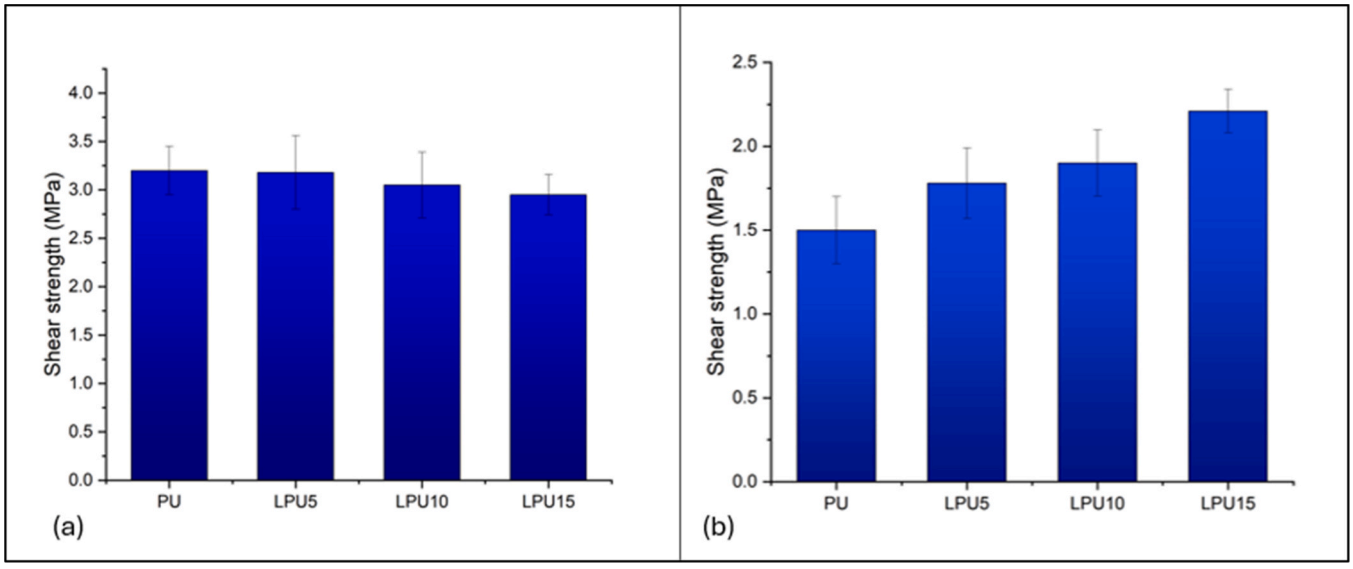


**Fig. 9.** Evaluation of shear strength for PU and LPU wood adhesives: (a) in dry condition and (b) in wet condition, highlighting the effect of KL incorporation on adhesive performance in different environmental states.

KL particles are embedded within the composite film, exhibiting good dispersion and distribution of KL in PU, contributing to a rough and irregular texture on the fractured surface. As the KL content increases in LPU10 and LPU15, the presence of agglomerated KL particles becomes more pronounced within the composite film. This leads to a rough fractured surface, characterized by larger and more prominent KL agglomerates dispersed within the PU matrix.

## 11. Evaluation of adhesive strength in dry and wet environments

The wood adhesive strength of PU and all LPU composite resins were evaluated by joining wooden blocks using PU and LPU composite adhesives and testing them in both dry and wet conditions [38,67,68]. The resulting images of the lap shear test are shown inFig. 9, and the digital images of wood fractures are presented in Fig. 10. It is clearly visible from Fig. 9a that the lap shear strength for PU in dry state is approximately 3.20 ± 0.15 MPa. However, incorporating 5 wt% KL into PU results in a shear strength of 3.18 ± 0.44 MPa. Additionally, all prepared LPU samples exhibit dose-dependent behavior, which is in line with earlier studies in the literature [38,67]. The incorporation of KL leads to a pronounced variation in the shear strength of the wood adhesive blocks. For example, increasing KL loadings in LPU from 5 to 10–15 wt %, leads to slightly decreased shear strength from 3.18 ± 0.44 MPa to 3.05 ± 0.34 – 2.95 ± 0.20 MPa, respectively. It is very important to note that the LPU composite resins with 5 wt% of KL exhibit optimal adhesion strength in the dry state, but with 10–15 wt% of KL the shear strength slightly decreases with increasing KL content. This slight decrease in LPU composites might be due to the interaction of hydrophilic wood surface with hydrophobic KL present in all LPU samples. As a result, the LPU resin may face difficulty establishing a comparatively stronger interaction with wood than PU in dry state [69,70].

The lap shear strength of PU and LPU polymer composite resins in a wet environment is shown in Fig. 9b. In the wet state, the lap shear strength of pure PU was 1.50 ± 0.20 MPa while with 5 wt% KL incorporation, the strength increased to 1.78 ± 0.25 MPa. Furthermore, as the KL content increased from 10 wt% to 15 wt% in LPU10 and LPU15, the lap shear strength rose to 1.90 ± 0.19 MPa and 2.21 ± 0.13 MPa, respectively. The results indicate that in the wet state, the LPU composite resins exhibited significantly better characteristics than pure PU. This might be due to the interaction of water molecules with the hydrophilic surface of wood, which is repelled by the hydrophobic KL molecules. This repulsion can significantly improve the composite resin's water resistance ability in aqueous conditions by directly enhancing the physical crosslinking [68,71]. Overall, the adhesion strength of wood is determined by its physico-chemical interlocking process [68]. The majority of the wood surfaces are made up of many micropores containing a large number of polar functional groups (hemicellulose, cellulose's –(OH)/hydroxyl groups) [72]. A strong secondary contact is thus established (H-bonding and van der Waals interaction) between the polar components of the applied adhesive and the cellulose equivalents (mostly the -OH group) of the wood surface, after the adhesive is applied on the wood surface and the adhesive diffuses into the micropores of the wood. As soon as the adhesive solidifies, the adhesion interaction progressively rises. Consequently, a mechanically rigid adhesive line is formed, when the applied composite resin becomes physically interlocked between the hardwood substrates. Therefore, during a lap-shear test, the robust adhesive interlocking holds the wood blocks together even under stress. Since the adhesive line's bonding strength is higher than the hardwood substrate's, separation generally occurs through wood failure (as observed from the digital photos inFig. 10) [67]. Although pure PU resin demonstrates good bonding strength with wooden blocks, all LPU composite samples incorporating KL exhibit a noticeable increase in adhesion strength in wet environment. It is noteworthy that our adhesive formulations show higher adhesive strength compared to the ASTM D4690 standard of urea-formaldehyde-resin for plywood adhesive requirement of 2.344 MPa under dry conditions [73]. Under wet conditions, however, the ASTM D4690 standard-defined minimum strength of 1.93 MPa was met by LPU10 and LPU15 as 1.90 ± 0.19 MPa and 2.21 ± 0.13 MPa, respectively, highlighting their potential for practical and commercial adhesive applications where moisture resistance is critical [70,73].

## 12. SEM analysis of fractured wood surface

To investigate the fracture mechanics of wood-adhesive joints, SEM analysis was conducted on the fractured surfaces of wood substrates bonded with PU and LPU composites under both dry and wet conditions.

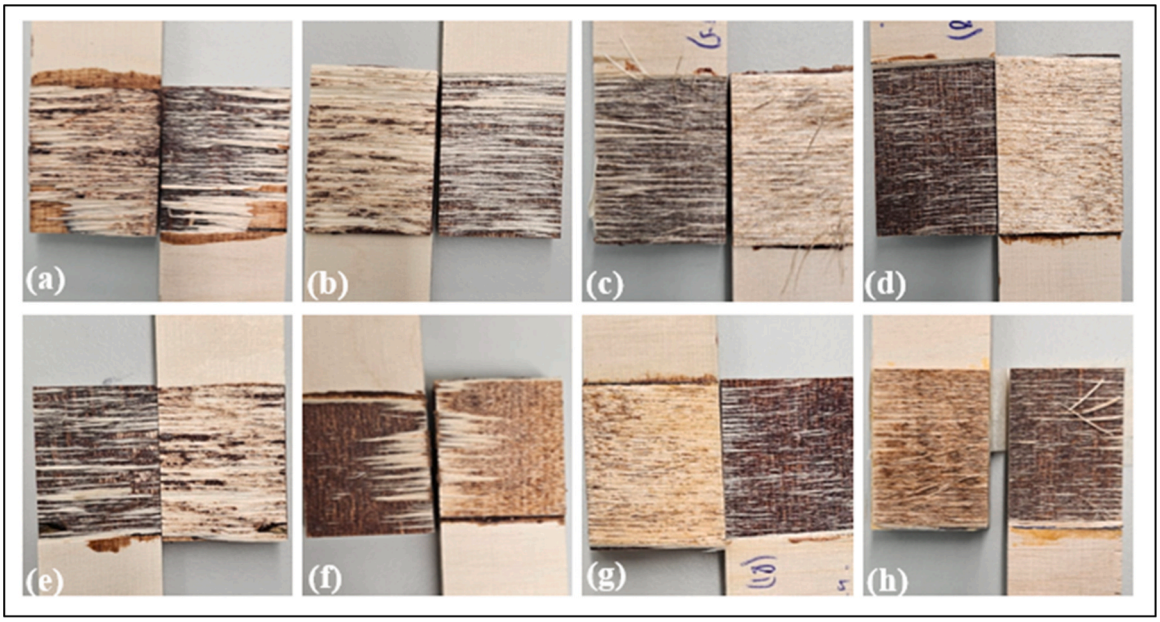


**Fig. 10.** Digital images of fractured wood adhesive joints bonded with PU and LPU adhesives: under dry conditions; (a) PU, (b) LPU5, (c) LPU10, and (d) LPU15; and under wet conditions; (e) PU, (f) LPU5, (g) LPU10, and (h) LPU15. The fractured surfaces reflect the effect of KL content and environmental exposure on adhesive integrity and bonding quality.

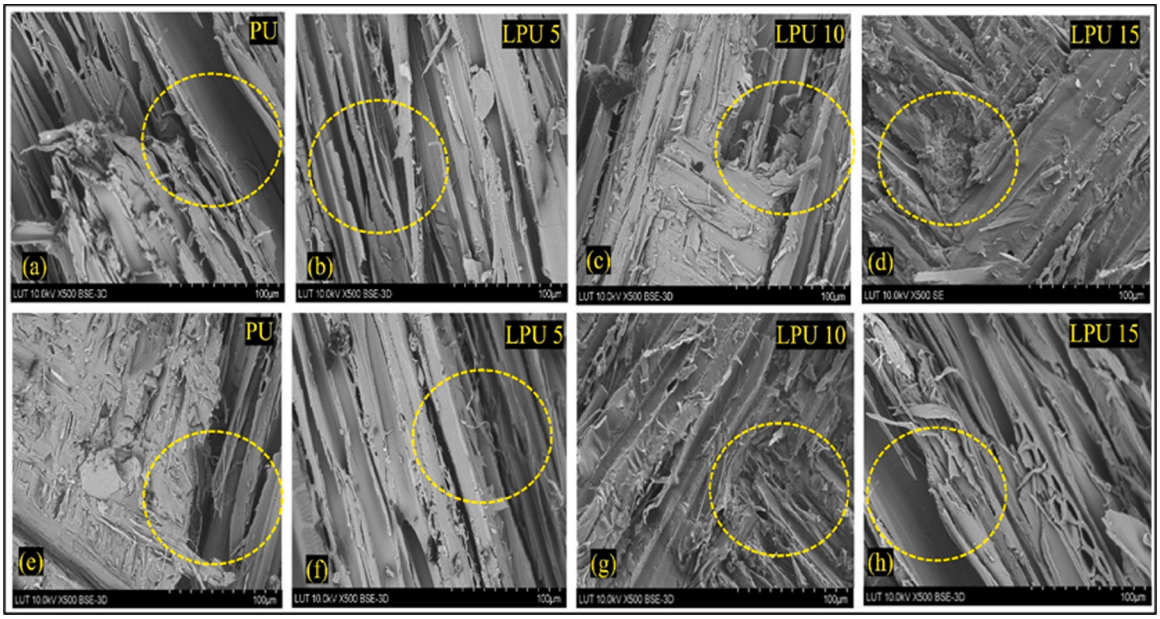


**Fig. 11.** SEM images of mechanically fractured wood surfaces bonded with PU and LPU adhesives: in dry condition; (a) PU, (b) LPU5, (c) LPU10, and (d) LPU15; in wet condition; (e) PU, (f) LPU5, (g) LPU10, and (h) LPU15. These images highlight morphological variations in interfacial adhesion and fracture behavior due to KL incorporation and environmental conditions.

In the dry state (Fig. 11a), the fractured surfaces of PU-bonded specimens showed that fracture propagation initiated from the wood lumens, indicating a strong adhesive bond with the wood. Similarly, SEM images of LPU composite-bonded substrates in the dry state (Figs. 11b-d) also showed fracture initiation from the wood layers, demonstrating a strong wood-adhesive interaction [71]. However, under wet conditions, distinct differences were observed. InFig. 11e (PU-bonded wood substrates), fracture initiation is primarily observed within the adhesive layer, although the wood lumens also display signs of failure. In contrast, SEM images of LPU composite resins in the wet state (Figs. 11f-h) reveal that fracture propagation originates from the wood lumens, supporting the presence of robust wood-adhesive interactions. These lumens appear to be torn across the bonded interface, with increasing KL content leading to deeper wood damage. This dose-dependent behavior suggests enhanced mechanical interlocking and adhesion strength in LPU composites [69]. The improved adhesive performance of LPU in wet conditions may be attributed to the intrinsic water resistance of KL, as well as the enhanced physico-mechanical interlocking between the LPU composite resin and the wood substrate.

## 13. Conclusion

In this research, we successfully synthesized and characterized novel polyurethane composites (LPU), incorporating kraft lignin (KL) as a bio-based additive alongside castor oil (CO) into the PU matrix. Comprehensive characterization using FTIR, WAXS, X-FESEM, and SS-CP-MAS $^{1}$ $^{3}$C NMR techniques confirmed successful integration of KL into the PU system. FTIR analysis revealed specific interactions between KL and the PU resin, while WAXS and FESEM demonstrated homogeneous dispersion of KL within the PU matrix. SS-CP-MAS $^{13}$C NMR further verified the chemical incorporation of KL-additive functional groups into the PU. The composites exhibited remarkable mechanical improvements, with LPU film containing 5 wt% KL showing a 125 % increase in tensile strength (8.10 ± 1.0 MPa) compared to pure PU (3.6 ± 1.50 MPa). As adhesives, LPU composites displayed superior performance, particularly under wet conditions, where LPU15 showed a 45 % enhancement in lap shear strength (2.19 ± 0.03 MPa) over pure PU (1.51 ± 0.31 MPa), attributed to hydrophobic nature of KL. Beyond mechanical properties, the incorporation of KL in PU also imparted significant bioactive functionalities. LPU10 and LPU15 demonstrated moderate antibacterial activity against both *E. coli* and *S. aureus* (MIC = 25 mg/mL), while DPPH assays revealed dose-dependent antioxidant capacity, with LPU15 exhibiting the highest radical scavenging activity. These findings establish the LPU composites as multifunctional, bio-based materials with enhanced mechanical properties, water resistance, and intrinsic bioactive functionalities, making them ideally suitable for diverse industrial applications, including adhesives (construction, automotive, marine), protective coatings (packaging, medical devices, agriculture films), and sustainable insulation foams. Subsequent research will focus on higher KL loadings (>15 wt%), conducting comprehensive environmental assessments (life cycle analysis, carbon footprint, biodegradability studies), and evaluating commercial viability through pilot-scale trials. This work represents an important step toward developing high-performance, sustainable alternatives to conventional petroleum-based PU, aligning with global circular economy objectives.

## CRediT authorship contribution statement

**Maham Arif:** Writing – review & editing, Writing – original draft, Visualization, Validation, Software, Resources, Project administration, Methodology, Investigation, Funding acquisition, Formal analysis, Data curation, Conceptualization. **Avishek Mallick Choudhury:** Visualization, Formal analysis, Data curation. **Aleezay Anjum Ahmed:** Writing – original draft, Software. **Vijay Singh Parihar:** Formal analysis, Data curation, Visualization, Writing – review & editing. **Md. Elias Uddin:** Visualization, Software. **Minna Kellomäki:** Software, Formal analysis. **Pralay Maiti:** Writing – review & editing, Software, Formal analysis. **Rama Layek:** Writing – review & editing, Writing – original draft, Supervision, Resources, Project administration, Funding acquisition, Formal analysis.

## Declaration of Generative AI and AI-assisted technologies in the writing process

The authors used ChatGPT to improve language and readability of the manuscript.

## Declaration of Competing Interest

The authors declare that they have no known competing financial interests or personal relationships that could have appeared to influence the work reported in this paper.

## Acknowledgments

Authors acknowledges the Fortum and Neste Foundation funding (grant number 20230051) for supporting doctoral research and Kollin säätiö foundation for biorefinery research at LUT University, Lahti campus, Finland.

## Data availability

Data will be made available on request.

## References

[1] P. Sikdar, T.M. Dip, A.K. Dhar, M. Bhattacharjee, M.S. Hoque, S.Bin Ali, Polyurethane (PU) based multifunctional materials: emerging paradigm for functional textiles, smart, and biomedical applications, John Wiley Sons Inc. (2022), https://doi.org/10.1002/app.52832.
[2] A. Das, P. Mahanwar, A brief discussion on advances in polyurethane applications, KeAi Commun. Co. (2020), https://doi.org/10.1016/j.aiepr.2020.07.002.
[3] A. Delavarde, et al., Sustainable polyurethanes: toward new cutting-edge opportunities, Elsevier Ltd (2024), https://doi.org/10.1016/j.progpolymsci.2024.101805.
[4] F.M. De Souza, P.K. Kahol, R.K. Gupta, Introduction to Polyurethane Chemistry, American Chemical Society, 2021, https://doi.org/10.1021/bk-2021-1380.ch001.
[5] J.O. Akindoyo, M.D.H. Beg, S. Ghazali, M.R. Islam, N. Jeyaratnam, A.R. Yuvaraj, Polyurethane types, synthesis and applications-a review, R. Soc. Chem. (2016), https://doi.org/10.1039/c6ra14525f.
[6] J. Datta, P. Kasprzyk, Thermoplastic polyurethanes derived from petrochemical or renewable resources: A comprehensive review, John Wiley Sons Inc. (2018), https://doi.org/10.1002/pen.24633.
[7] P.M. Paraskar, M.S. Prabhudesai, V.M. Hatkar, R.D. Kulkarni, Vegetable oil based polyurethane coatings – A sustainable approach: a review, Prog. Org. Coat. 156 (2021) 106267, https://doi.org/10.1016/J.PORGCOAT.2021.106267.
[8] A. Arias, E. Entrena-Barbero, G. Feijoo, M.T. Moreira, Sustainable non-isocyanate polyurethanes bio-adhesives for engineered wood panels are revealed as promising candidates to move from formaldehyde-based alternatives, J. Environ. Chem. Eng. 10 (1) (2022), https://doi.org/10.1016/j.jece.2021.107053.
[9] M. Abdollahi, M. Pourmahdi, A.R. Nasiri, Synthesis and characterization of lignosulfonate/acrylamide graft copolymers and their application in environmentally friendly water- based drilling fluid, J. Pet. Sci. Eng. 171 (2018) 484–494, https://doi.org/10.1016/j.petrol.2018.07.065.
[10] A. Tenorio-Alfonso, M.L. Pizarro, M.C. Sánchez, J.M. Franco, Assessing the rheological properties and adhesion performance on different substrates of a novel green polyurethane based on castor oil and cellulose acetate: a comparison with commercial adhesives, Int J. Adhes. Adhes. 82 (2018) 21–26, https://doi.org/10.1016/j.ijadhadh.2017.12.012.
[11] A. Delavarde, et al., Sustainable polyurethanes: toward new cutting-edge opportunities, Elsevier Ltd (2024), https://doi.org/10.1016/j.progpolymsci.2024.101805.
[12] G. La Torre, T. Vitello, R.A. Cocchiara, C. Della Rocca, Relationship between formaldehyde exposure, respiratory irritant effects and cancers: a review of reviews, Elsevier B. V. (2023), https://doi.org/10.1016/j.puhe.2023.03.009.
[13] H. Sheikhy, M. Shahidzadeh, B. Ramezanzadeh, F. Noroozi, Studying the effects of chain extenders chemical structures on the adhesion and mechanical properties of a polyurethane adhesive, J. Ind. Eng. Chem. 19 (6) (2013) 1949–1955, https://doi.org/10.1016/j.jiec.2013.03.008.
[14] P.H. Chen, et al., Synthesis and properties of transparent thermoplastic segmented polyurethanes, Adv. Polym. Technol. 26 (1) (2007) 33–40, https://doi.org/10.1002/adv.20086.
[15] B.L. Xue, J.L. Wen, R.C. Sun, Lignin-based rigid polyurethane foam reinforced with pulp fiber: Synthesis and characterization, ACS Sustain Chem. Eng. 2 (6) (2014) 1474–1480, https://doi.org/10.1021/sc5001226.
[16] X. Li, X. Chen, S. Zhang, Y. Yin, C. Wang, UV-resistant transparent lignin-based polyurethane elastomer with repeatable processing performance, Eur. Polym. J. 159 (2021), https://doi.org/10.1016/j.eurpolymj.2021.110763.
[17] X. Ma, J. Chen, J. Zhu, N. Yan, Lignin-Based Polyurethane: Recent Advances and Future Perspectives, WileyVCH Verl. (2021), https://doi.org/10.1002/marc.202000492.
[18] A. Cassales, L.A. Ramos, E. Frollini, Synthesis of bio-based polyurethanes from Kraft lignin and castor oil with simultaneous film formation, Int J. Biol. Macromol. 145 (2020) 28–41, https://doi.org/10.1016/j.ijbiomac.2019.12.173.
[19] J.R. Gouveia, C.L. da Costa, L.B. Tavares, D.J. Dos Santos, Synthesis of lignin-based polyurethanes: a mini-review, Bentham Sci. Publ. (2019), https://doi.org/10.2174/1570193X15666180514125817.
[20] V.K. Thakur, M.K. Thakur, P. Raghavan, M.R. Kessler, Progress in green polymer composites from lignin for multifunctional applications: a review, ACS Sustain Chem. Eng. 2 (5) (2014) 1072–1092, https://doi.org/10.1021/sc500087z.
[21] Y. Zhang, J. Liao, X. Fang, F. Bai, K. Qiao, L. Wang, Renewable high-performance polyurethane bioplastics derived from lignin-poly(ε-caprolactone), ACS Sustain Chem. Eng. 5 (5) (2017) 4276–4284, https://doi.org/10.1021/acssuschemeng.7b00288.
[22] J. Sternberg, S. Pilla, Materials for the biorefinery: high bio-content, shape memory Kraft lignin-derived non-isocyanate polyurethane foams using a non-toxic protocol, Green. Chem. 22 (20) (2020) 6922–6935, https://doi.org/10.1039/d0gc01659d.
[23] F.R. Vieira, N. Gama, S. Magina, A. Barros-Timmons, D.V. Evtuguin, P.C.O. R. Pinto, Polyurethane adhesives based on oxyalkylated kraft lignin, Polymers 14 (23) (2022), https://doi.org/10.3390/polym14235305.
[24] P. Cinelli, I. Anguillesi, A. Lazzeri, Green synthesis of flexible polyurethane foams from liquefied lignin, *Eur. Polym. J.* (2013) 1174–1184, https://doi.org/10.1016/j.eurpolymj.2013.04.005.
[25] X. Ma, J. Chen, J. Zhu, N. Yan, Lignin-based polyurethane: recent advances and future perspectives, WileyVCH Verl. (2021), https://doi.org/10.1002/marc.202000492.
[26] M. Xu, et al., Preparation and antibacterial study of waterborne polyurethane modified with lysine and quaternary ammonium salt, N. J. Chem. 47 (22) (2023) 10715–10726, https://doi.org/10.1039/d3nj01200j.
[27] Y. Wang, et al., Fabrication of litchi-like lignin/zinc oxide composites with enhanced antibacterial activity and their application in polyurethane films, J. Colloid Interface Sci. 594 (2021) 316–325, https://doi.org/10.1016/j.jcis.2021.03.033.
[28] A. Boubakri, N. Guermazi, K. Elleuch, H.F. Ayedi, Study of UV-aging of thermoplastic polyurethane material, Materials Science Engineering A 527 (7–8) (2010) 1649–1654, https://doi.org/10.1016/j.msea.2010.01.014.
[29] K. Gorna, S. Gogolewski, Biodegradable polyurethanes for implants. II. In vitro degradation and calcification of materials from poly(ε-caprolactone)-poly(ethylene oxide) diols and various chain extenders, J. Biomed. Mater. Res 60 (4) (2002) 592–606, https://doi.org/10.1002/jbm.10100.
[30] S. Chandra, N. Karak, Environmentally friendly polyurethane dispersion derived from dimer acid and citric acid, ACS Sustain Chem. Eng. 6 (12) (2018) 16412–16423, https://doi.org/10.1021/acssuschemeng.8b03474.
[31] L.D. Antonino, I. Sumerskii, A. Potthast, T. Rosenau, M.I. Felisberti, D.J. dos Santos, Lignin-based polyurethanes from the blocked isocyanate approach: synthesis and characterization, ACS Omega 8 (30) (2023) 27621–27633, https://doi.org/10.1021/acsomega.3c03422.
[32] L.B. Tavares, C.V. Boas, G.R. Schleder, A.M. Nacas, D.S. Rosa, D.J. Santos, Bio-based polyurethane prepared from Kraft lignin and modified castor oil, Express Polym. Lett. 10 (11) (2016) 927–940, https://doi.org/10.3144/expresspolymlett.2016.86.
[33] H.J. Kim, X. Jin, J.W. Choi, Investigation of bio-based rigid polyurethane foams synthesized with lignin and castor oil, Sci. Rep. 14 (1) (2024), https://doi.org/10.1038/s41598-024-64318-8.
[34] O. Xosocotla, B. Campillo, H. Martínez, M.del P. Rodríguez-Rojas, R. Campos, V. Bustos-Terrones, Modification of polyurethane/graphene oxide with dielectric barrier plasma treatment for proper coating adhesion on fiberglass, Coatings 15 (4) (2025), https://doi.org/10.3390/coatings15040411.
[35] M.P. Weinstein, 2019, Performance standards for antimicrobial susceptibility testing. Clinical and Laboratory Standards Institute.
[36] Y. Fang, et al., Recyclable polyurethane from castor oil based on dynamic disulfide bonds and multiple hydrogen bonds as adhesive and photothermal conversion materials, Ind. Crops Prod. 222 (2024), https://doi.org/10.1016/j.indcrop.2024.120027.
[37] A. Tenorio-Alfonso, M.L. Pizarro, M.C. Sánchez, J.M. Franco, Assessing the rheological properties and adhesion performance on different substrates of a novel green polyurethane based on castor oil and cellulose acetate: a comparison with commercial adhesives, Int J. Adhes. Adhes. 82 (2018) 21–26, https://doi.org/10.1016/j.ijadhadh.2017.12.012.
[38] T. Ghosh, T. Elo, V.S. Parihar, P. Maiti, R. Layek, Poly (itaconic acid) functionalized lignin/polyvinyl acetate composite resin with improved sustainability and wood adhesion strength, Ind. Crops Prod. 187 (2022), https://doi.org/10.1016/j.indcrop.2022.115299.
[39] Test Method for Strength Properties of Adhesives in Plywood Type Construction in Shear by Tension Loading, ASTM International, West Conshohocken, PA, Apr. 01, 2020, https://doi.org/10.1520/D0906-20.
[40] M.N. Mohamad Ibrahim, N. Zakaria, C.S. Sipaut, O. Sulaiman, R. Hashim, Chemical and thermal properties of lignins from oil palm biomass as a substitute for phenol in a phenol formaldehyde resin production, Carbohydr. Polym. 86 (1) (2011) 112–119, https://doi.org/10.1016/J.CARBPOL.2011.04.018.
[41] I.S. Ristić, et al., The properties of polyurethane hybrid materials based on castor oil, Mater. Chem. Phys. 132 (1) (2012) 74–81, https://doi.org/10.1016/j.matchemphys.2011.10.053.
[42] L.B. Tavares, C.V. Boas, G.R. Schleder, A.M. Nacas, D.S. Rosa, D.J. Santos, Bio-based polyurethane prepared from Kraft lignin and modified castor oil, Express Polym. Lett. 10 (11) (2016) 927–940, https://doi.org/10.3144/expresspolymlett.2016.86.
[43] F.de Oliveira, E.C. Ramires, E. Frollini, M.N. Belgacem, Lignopolyurethanic materials based on oxypropylated sodium lignosulfonate and castor oil blends, Ind. Crops Prod. 72 (2015) 77–86, https://doi.org/10.1016/J.INDCROP.2015.01.023.
[44] Y. Kurimoto, M. Takeda, A. Koizumi, S. Yamauchi, S. Doi, Y. Tamura, Mechanical properties of polyurethane ®lms prepared from lique®ed wood with polymeric MDI 74 (2) (2000) 151–157, https://doi.org/10.1016/S0960-8524(00)00009-2.

[45] S. Hirose, T. Hatakeyama, Y. Izuta, H. Hatakeyama, TG-ftir studies on lignin-based polycaprolactones, J. Therm. Anal. Calor. 70 (2002) 853–860, https://doi.org/10.1023/A:1022212421525.
[46] Y. Meng, et al., Understanding the local structure of disordered carbons from cellulose and lignin, Wood Sci. Technol. 55 (3) (2021) 587–606, https://doi.org/10.1007/s00226-021-01286-6.
[47] I.S. Stefanović, et al., Composition-property relationship of polyurethane networks based on polycaprolactone diol, Polym. Bull. 78 (12) (2021) 7103–7128, https://doi.org/10.1007/s00289-020-03473-0.
[48] A. GÜNEY, A. KIZILTAY, N. HASIRCI, T. ENDOĞAN TANIR, Synthesis and characterization of polycaprolactone-based segmented polyurethanes, Turk. J. Chem. 43 (2) (2019) 452–463, https://doi.org/10.3906/kim-1801-44.
[49] M. Culebras, A. Beaucamp, Y. Wang, M.M. Clauss, E. Frank, M.N. Collins, Biobased structurally compatible polymer blends based on lignin and thermoplastic elastomer polyurethane as carbon fiber precursors, ACS Sustain Chem. Eng. 6 (7) (2018) 8816–8825, https://doi.org/10.1021/acssuschemeng.8b01170.
[50] D.T. Okamoto, S.L. Cooper, T.W. Root, NMR Investigation of a Poly(urethane-urea) System, Macromolecules 25 (3) (1992) 1068–1073, https://doi.org/10.1021/ma00029a009.
[51] E.I. Evstigneyev, A.S. Mazur, A.V. Kalugina, A.V. Pranovich, A.V. Vasilyev, Solid-state 13C CP/MAS NMR for Alkyl-O-aryl bond determination in lignin preparations, J. Wood Chem. Technol. 38 (2) (2018) 137–148, https://doi.org/10.1080/02773813.2017.1393436.
[52] S. Gómez-Fernández, L. Ugarte, T. Calvo-Correas, C. Peña-Rodríguez, M. A. Corcuera, A. Eceiza, Properties of flexible polyurethane foams containing isocyanate functionalized kraft lignin, Ind. Crops Prod. 100 (2017) 51–64, https://doi.org/10.1016/J.INDCROP.2017.02.005.
[53] M. Wysokowski, et al., Modification of chitin with kraft lignin and development of new biosorbents for removal of cadmium(II) and nickel(II) ions, Mar. Drugs 12 (4) (2014) 2245–2268, https://doi.org/10.3390/md12042245.
[54] W. Kolodziejski, J.S. Frye, Carbon-13 nuclear magnetic resonance spectrometry with cross polarization and magic-angle spinning for analysis of lodgepole pine wood (and G. E. Maclel), Anal. Chem. 54 (8) (1982) 1419–1424, https://doi.org/10.1021/ac00245a035.
[55] L.J. Marshall, et al., Preparation of thermally curable materials using lignin extracted from sawmill co-product, RSC Sustain. 3 (2025) 1870–1885, https://doi.org/10.1039/d4su00767k.
[56] T. Asakura, Y. Ibe, T. Jono, A. Naito, Structure and dynamics of biodegradable polyurethane-silk fibroin composite materials in the dry and hydrated states studied using 13C solid-state NMR spectroscopy, Polym. Degrad. Stab. 190 (2021) 109645, https://doi.org/10.1016/J.POLYMDEGRADSTAB.2021.109645.
[57] W.-H. Ku, et al., Solid-State High-Resolution $^{13}$C NMR studies on the structure-property relationship of simultaneous interpenetrating networks from castor oil based polyurethane and polystyrene, Macromolecules 24 (16) (1991) 4605–4610, https://doi.org/10.1021/ma00016a020.
[58] Y.Z. Wang, Y.C. Hsu, R.R. Wu, H.M. Kao, Synthesis and structure properties of polyurethane based conducting copolymer I. $^{13}$C NMR analysis, Synth. Met 132 (2) (2003) 151–160, https://doi.org/10.1016/S0379-6779(02)00207-2.
[59] S.E. Klein, A. Alzagameem, J. Rumpf, I. Korte, J. Kreyenschmidt, M. Schulze, Antimicrobial activity of lignin-derived polyurethane coatings prepared from unmodified and demethylated lignins, Coatings 9 (8) (2019), https://doi.org/10.3390/coatings9080494.
[60] L.B. Tavares, N.M. Ito, M.C. Salvadori, D.J. dos Santos, D.S. Rosa, PBAT/kraft lignin blend in flexible laminated food packaging: peeling resistance and thermal degradability, Polym. Test. 67 (2018) 169–176, https://doi.org/10.1016/j.polymertesting.2018.03.004.
[61] J. Domínguez-Robles, Á. Cárcamo-Martínez, S.A. Stewart, R.F. Donnelly, E. Larrañeta, M. Borrega, Lignin for pharmaceutical and biomedical applications – Could this become a reality? Elsevier B. V. (2020) https://doi.org/10.1016/j.scp.2020.100320.
[62] V.K. Thakur, M.K. Thakur, Recent advances in green hydrogels from lignin: a review, Int J. Biol. Macromol. 72 (2015) 834–847, https://doi.org/10.1016/J.IJBIOMAC.2014.09.044.
[63] S.R. Yearla, K. Padmasree, Preparation and characterisation of lignin nanoparticles: evaluation of their potential as antioxidants and UV protectants, J. Exp. Nanosci. 11 (4) (2016) 289–302, https://doi.org/10.1080/17458080.2015.1055842.
[64] L.M. Sanchez, et al., Antioxidant cellulose nanofibers/lignin-based aerogels: a potential material for biomedical applications, Chem. Biol. Technol. Agric. 10 (1) (2023), https://doi.org/10.1186/s40538-023-00438-z.
[65] M. Farooq, T. Zou, G. Riviere, M.H. Sipponen, M. Österberg, Strong, ductile, and waterproof cellulose nanofibril composite films with colloidal lignin particles, Biomacromolecules 20 (2) (2019) 693–704, https://doi.org/10.1021/acs.biomac.8b01364.
[66] M.S. Dwijaya, D.A. Setiaji, J.H. Mustafa, M. Chalid, Lignin Effect to Synthesis of the Hybrid Polyurethane. in *IOP Conference Series: Materials Science and Engineering*, Institute of Physics Publishing, Mar. 2020, https://doi.org/10.1088/1757-899X/740/1/012059.
[67] A. Kaboorani, B. Riedl, P. Blanchet, M. Fellin, O. Hosseinaei, S. Wang, Nanocrystalline cellulose (NCC): a renewable nano-material for polyvinyl acetate (PVA) adhesive, Eur. Polym. J. 48 (11) (2012) 1829–1837, https://doi.org/10.1016/j.eurpolymj.2012.08.008.
[68] T. Todorovic, E. Norström, F. Khabbaz, J. Brücher, E. Malmström, L. Fogelström, A fully bio-based wood adhesive valorising hemicellulose-rich sidestreams from the pulp industry, Green. Chem. 23 (9) (2021) 3322–3333, https://doi.org/10.1039/d0gc04273k.
[69] R.V. Gadhave, P. S. Kasbe, P.A. Mahanwar, P.T. Gadekar, Synthesis and characterization of lignin-polyurethane based wood adhesive, Int J. Adhes. Adhes. 95 (2019), https://doi.org/10.1016/j.ijadhadh.2019.102427.
[70] B.B. Adhikari, P. Appadu, V. Kislitsin, M. Chae, P. Choi, D.C. Bressler, Enhancing the adhesive strength of a plywood adhesive developed from hydrolyzed specified risk materials, Polymers 8 (8) (2016), https://doi.org/10.3390/polym8080285.
[71] Z. Wang, Z. Li, Z. Gu, Y. Hong, L. Cheng, Preparation, characterization and properties of starch-based wood adhesive, Carbohydr. Polym. 88 (2) (2012) 699–706, https://doi.org/10.1016/j.carbpol.2012.01.023.
[72] T. Ghosh, B. Voit, N. Karak, Polystyrene/thermoplastic polyurethane interpenetrating network-based nanocomposite with high-speed, thermo-responsive shape memory behavior, Polymers 200 (2020) 122575, https://doi.org/10.1016/J.POLYMER.2020.122575.
[73] Specification for Urea-Formaldehyde Resin Adhesives, ASTM International, West Conshohocken, PA, Oct. 01, 2012, 10.1520/D4690-12.